RanBP2/Nup358 enhances RNAi activity by sumoylating and stabilizing Argonaute 1

Qingtang Shen[1], Mathew Truong[1], Kohila Mahadevan[1], Yifan E. Wang[1], Jing Ze Wu[1], Alexander F. Palazzo[1,2]

1- Department of Biochemistry, University of Toronto, Toronto, ON, Canada

2- Corresponding author: alex.palazzo@utoronto.ca.

ABSTRACT

RanBP2/Nup358 is one of the main components of the cytoplasmic filaments of the nuclear pore complex. Four separate missense mutations in RanBP2 cause Acute Necrotizing Encephalopathy 1 (ANE1), which manifests as a sharp rise in cytokine production after common viral infections such as influenza and parainfluenza. Infection in these individuals often leads to seizures, coma and a high rate of mortality. However, how RanBP2 and its ANE1-associated mutations affect cytokine production is not well understood. Here we report that RanBP2 represses the translation of the *interleukin-6 (IL6*) mRNA, which encodes a cytokine that is aberrantly up-regulated in ANE1. In particular, the SUMO E3-ligase activity of RanBP2 and the *Let7* miRNA binding site within the *IL6* 3′ untranslated region (UTR) are required for this repression, suggesting that sumoylation promotes efficient miRNA-based silencing. Furthermore, our data indicates that RanBP2-dependent sumoylation of the argonaute protein AGO1 inhibits its ubiquitination and its degradation, and that overexpression of AGO1 partially restores the repression of IL6 in cells that are defective in RanBP2-dependent sumoylation. Collectively, these results support a model whereby RanBP2 promotes the sumoylation of AGO1, which stabilizes it, and ultimately enhances the miRNA-mediated suppression of mRNAs such as *IL6*.

INTRODUCTION

Ran-binding protein 2 (RanBP2), also known as Nucleoporin 358 KDa (Nup358), is one of the main components of the cytoplasmic filaments of the nuclear pore complex (NPC) (Hoelz *et al*, 2011). It has been implicated in regulating mRNA metabolism (Forler *et al*, 2004; Grünwald & Singer, 2010; Mahadevan *et al*, 2013; Palazzo & Truong, 2016), and has an SUMO E3-ligase domain that post-translationally modifies several proteins (Pichler *et al*, 2002). Previously, we found that RanBP2 was required for the efficient translation of mRNAs that contain signal sequence coding regions (SSCRs), which code for short hydrophobic polypeptides and are found at the 5′ end of the open reading frame (ORF) of most secretory and membrane-bound proteins (Mahadevan *et al*, 2013). The majority of SSCRs in vertebrates are depleted of adenines, are enriched in GC-motifs and are present in the first exon (Palazzo *et al*, 2007, 2013; Cenik *et al*, 2011, 2017). Importantly, human RanBP2 contains eight zinc fingers that directly bind to adenine-depleted SSCRs (Mahadevan *et al*, 2013). Moreover, the ability of RanBP2 to promote translation is dependent on its zinc fingers and the presence of an adenine-depleted SSCR (Mahadevan *et al*, 2013). Overall our results suggest that upon the completion of nuclear export, mRNAs that contain adenine-depleted SSCRs directly interact with RanBP2 through its zinc fingers, and that this interaction likely modifies proteins that are associated with the mRNA in order to potentiate the translation of these mRNAs (Mahadevan *et al*, 2013; Palazzo *et al*, 2013; Palazzo & Truong, 2016).

Mutations in RanBP2 has also been associated with pathology. In particular, four separate missense mutations in the N-terminal region of RanBP2 (T585M, T653I, I656V, and T681C) are genetic risk factors for a pediatric neurological disease called acute-necrotizing

encephalopathy (ANE1) (Neilson *et al*, 2009; Sell *et al*, 2016). 40% of individuals with one of these dominant mutations secrete excessive amounts of cytokines (known as a "cytokine storm") in response to influenza infection (Kansagra & Gallentine, 2011; Tisoncik *et al*, 2012; Singh *et al*, 2015). Generally, the massive secretion of cytokines include pro-inflammatory cytokines such as IL6, TNFα, IL10, IFNγ, sTNFα receptor, and IL15 (Ichiyama *et al*, 1998, 2003a, 2003b; Ito *et al*, 1999; Akiyoshi *et al*, 2006; Tabarki *et al*, 2013; Wu *et al*, 2015) (Table 1). The resulting elevated levels of cytokines infiltrate into the cerebral spinal fluid, causing neuropathology, seizures, coma and a high rate of mortality. Those who survive often suffer from long-term neurological damage. However, how RanBP2 contributes to the overproduction of ANE1-associated cytokines remains unclear.

The cytokine that has been best documented to be upregulated during ANE1 is IL6 (Table 1). The expression of this cytokine has been the subject of much investigation. One of the key ways in which IL6 is regulated is by the *Let7* miRNA, which recognizes one binding site in the 3′ untranslated region (UTR) of the *IL6* mRNA (Iliopoulos *et al*, 2009; Schulte *et al*, 2011). Indeed, many infections are known to modulate the expression of *Let7* miRNA family members and *Let7* modulates the inflammatory response (Iliopoulos *et al*, 2009; Schulte *et al*, 2011; Ma *et al*, 2012; Mazumder *et al*, 2013; Makkoch *et al*, 2016; Lin *et al*, 2017; Brennan *et al*, 2017). miRNAs associate with the RNA Induced Silencing Complex (RISC) to silence their targets, and the main component of this complex, the argonaute proteins, are regulated by post-translational modifications, such as ubiquitination and sumoylation, which in turn affect their activity and stability (Sahin *et al*, 2014; Derrien & Genschik, 2014; Josa-Prado *et al*, 2015; Chinen & Lei, 2017; Nayak *et al*, 2018; Kobayashi *et al*, 2018). Interestingly, a recent report indicates that

RanBP2 is required for *Let7* mediated gene silencing (Sahoo *et al*, 2017). These observations suggest that RanBP2 might impact the translation of the *IL6* mRNA by post-translational regulation of argonaute proteins.

Here we present evidence that RanBP2 promotes the *Let7*-mediated suppression of IL6 protein production by sumoylating AGO1, which antagonizes AGO1 ubiquitination and thus promotes its stability and its ability to translationally silence the *IL6* mRNA.

RESULTS

Most ANE1-associated cytokine genes have SSCRs that contain adenines and have low 5IMP scores

Previously, we found that RanBP2 potentiates the translation of mRNAs that contain adenine-depleted SSCRs at the beginning of their ORF (Mahadevan *et al*, 2013). Indeed these SSCRs tend to have long tracts of adenine-depleted sequence (Palazzo *et al*, 2007). Moreover, genes that contain adenine-depleted SSCRs tend to lack introns in their 5′UTRs, when compared to other genes in the human genome (Cenik *et al*, 2011). As a result, there are typically no introns upstream of adenine-depleted SSCRs, thus placing these elements within the first exon at rates that are higher than expected (Cenik *et al*, 2011). Genes that contain adenine-depleted SSCRs are also associated with a variety of other features in the 5′ end of the ORF (e.g., presence of certain GC-rich motifs, enhanced presence of N1-methyladenosine), which are also associated with a lack of introns in their 5′UTR (Cenik *et al*, 2017). Previously, we used machine learning to evaluate the 5′ end of ORFs for these features which are summed up into a 5′UTR intron minus prediction (5IMP) score (Cenik *et al*, 2017).

Since ANE1-associated cytokines (see Table 1) are produced from mRNAs that contain SSCRs, we decided to evaluate whether they are also depleted of adenines and have high 5IMP scores. Of note, most of these mRNAs are produced from genes that lack introns in their 5′UTRs (Table 1). Despite this, almost all ANE1-associated cytokines had very small adenine-less tracts when compared to other SSCR-containing genes that lacked introns in their 5′UTRs ("5UI-") from the human genome (Figure 1A). Indeed, the length of their longest adenine-less tract was on par with non-SSCR containing genes and intergenic sequences (Figure 1A), strongly indicating that

there is no selection for adenine-depletion in most ANE1-associated cytokine genes. One exception was IL6, which had a relatively long adenine-less tract. When 5IMP scores were evaluated, all ANE1-associated cytokines, including IL6, had low scores (<5) when compared to other SSCR-containing genes that lack 5′UTR introns ("SSCR 5UI-") where a significant fraction have scores greater than 7 (Figure 1B).

From these results we conclude that the sequence composition of SSCRs from ANE1-associated cytokine mRNAs do not have the features that are normally associated with mRNAs whose translation is upregulated by RanBP2.

RanBP2 inhibits the translation of an *IL6-HA* reporter mRNA

Of all the cytokines overproduced in ANE1-patients, IL6 has been the best documented (Table 1). We thus depleted RanBP2 using lentiviral delivered shRNAs (Figure 2A) and examined the expression of a C-terminally tagged IL6 expressed off of a transfected plasmid. Unexpectedly, we found that RanBP2-depletion resulted in a ~12 fold increase in intracellular IL6-HA when compared to control cells (Figure 2B-C). This was true of both intracellular and secreted IL6-HA (Figure 2D). This is in stark contrast to the expression of insulin whose mRNA has an adenine-depleted SSCR and a high 5IMP score, and requires RanBP2 for its efficient translation (Figure 2B-C) which is consistent from our previous findings (Mahadevan *et al*, 2013). The expression of *βglobin-HA* mRNA, which lacks an SSCR, was unaffected by RanBP2-depletion (Figure 2B-C).

The increase in IL6-HA protein synthesis was not due to changes in the total level *IL6* mRNA (Figure 2E-F), or to changes in the distribution of *IL6* mRNA between the cytoplasm and the nucleus (Figure 2G-H). Previous studies have demonstrated that splicing can potentiate the efficiency of translation (Nott *et al*, 2004), and the main *IL6* isoform has four introns. However, versions of the IL6 reporter that either contained the endogenous first intron (*IL6-1i*), or the intron of *fushi tarazu* mRNA (*ftz*), at the first intron site (*IL6-1f*) still produced more protein after RanBP2-depletion, indicating that this effect is independent of splicing (Figure S1A-C).

From these results, and from the results of our polysome profiling (see below), we conclude that RanBP2 inhibits IL6-HA protein production from a transfected reporter construct. As RanBP2-depletion did not affect the levels or the cytoplasmic/nuclear distribution of the reporter mRNA, we concluded that RanBP2 inhibits the translation of *IL6-HA* mRNA.

The SUMO E3-ligase domain of RanBP2 is required for the repression of IL6

Next, we investigated whether the SUMO E3-ligase activity of RanBP2 is required to inhibit the translation of the *IL6* mRNA. We used CRISPR/Cas9 with a specific guide RNA ("gRNA-dE3-1") to target the E3 domain of RanBP2 in U2OS cells (Figure 3A-B). We obtained a clone, called RanBP2 dead E3 (hereafter referred to as RanBP2-dE3), where one copy of the gene ("f1"; Figure 3A-D) had a 45 base pair (bp) deletion just downstream from the targeted region (i.e., the guide RNA Protospacer Adjacent Motif "PAM" site) that eliminated 15 amino acids in the SUMO E3-ligase domain, and where the second copy ("f2"; Figure 3A-D) had a 356 bp deletion which eliminated the remaining part of exon 21 and a portion of the following intronic sequence. We reasoned that the splicing of mRNAs generated from the f2 copy would produce a

mature mRNA that contains premature stop codons and thus should be eliminated by nonsense-mediated decay (NMD). Thus, we inferred that the cell line only produces protein from the f1 copy of the gene, which should lack a portion of the E3 domain. The E3 domain not only binds to Ubc9, which is the only known SUMO E2-ligase in humans, but also to SUMO-RanGAP1 (Saitoh *et al*, 1997). In agreement with this, the nuclear rim localization of RanGAP1 was disrupted in RanBP2-dE3 cells (Figure 3E) despite the fact that the mutant protein was still at the nuclear rim (Figure S2A). RanBP2-dE3 cells also had significantly decreased levels of RanBP2 protein, although this appeared to vary greatly between experiments (for example compare levels of RanBP2 in RanBP2-dE3 cells in Figure 3F and H), and had almost no detectable SUMO-conjugated RanGAP1 (SUMO-RanGAP1) (Figure 3F, 3H). Importantly, when RanBP2-dE3 cells were transfected with *IL6-⊿i-HA* or *IL6-1i-HA*, these cells had significantly elevated IL6-HA protein expression over control cells (Figure 3F-I). Note that co-transfected Histone1-GFP ("H1B-GFP") expression was similar in both cell lines (Figure 3F, 3H) indicating that there wasn't a general alteration in mRNA translation. Confirming that the effect on IL6 expression was due to a decrease in translation, we fractionated lysates from unmodified and RanBP2-dE3 U2OS cells on a sucrose gradient (Figure 3J) and assessed the distribution of mRNA by RT-qPCR (Figure 3K-L). We found that *IL6-HA* mRNA was shifted towards the light polysome fraction in mutant cells (Figure 3K). Meanwhile, the distribution of *α-tubulin* mRNA remained unaffected (Figure 3L). These data indicate that either the SUMO E3-ligase activity, or high levels of RanBP2, is required for the translational repression of the *IL6* mRNA.

To validate our findings, we also generated a RanBP2 sumoylation-deficient mutant in HAP1 cells. As these are haploid, we only have to modify the single copy of the *RanBP2* gene.

Using a similar strategy as described above for RanBP2-dE3 generation, we isolated a mutant HAP1 clone called RanBP2-E3 insertion mutant (hereafter referred to as RanBP2-E3 ins), which had a 51 bp (17 amino acids) insertion into the middle of the E3 domain (Figure 4A-B). Although RanBP2-E3 ins had no effect on RanBP2 protein level, it eliminated RanGAP1 sumoylation (Figure 4C). As we had observed in U2OS cells, expression of IL6-HA protein from the *IL6-1i-HA* reporter was higher in RanBP2-E3 ins cells than control HAP1 cells, when normalized to H1B-GFP expression (Figure 4C-D).

Taken together, these results demonstrate that the SUMO-E3 domain of RanBP2 is required to repress IL6-HA reporter protein production in cells.

RanBP2 with ANE1-associated mutations rescues the translational repression of the *IL6-HA* reporter mRNA

To evaluate the effect of the ANE1 mutant on the suppression of IL6 production, we isolated a clone of RanBP2-dE3 U2OS cells that stably expressed an N-terminal GFP-tagged RanBP2 bearing 3 of the ANE1 mutations (T585M, T653I, and I656V). This mutant localized to the nuclear rim (Figure S2B) and rescued IL6-HA repression in RanBP2-dE3 cells (Figure 3F-G), although it only partially restored SUMO-RanGAP1 (Figure 3F). It should be noted that the expression level of this protein was low (Figure 3F), suggesting that low levels of the SUMO E3-ligase activity is sufficient for RanBP2 to suppress IL6 expression.

From these results we conclude that since only low levels of the triple ANE1 mutant rescued the suppression of IL6-HA, it is unlikely that RanBP2-dE3 cells are unable to repress IL6

due to low levels of RanBP2. Furthermore, our results also indicate that the primary defect of the ANE1 mutations is not the general misregulation of IL6 expression. However, it remains possible that the ANE1 mutations may impact the expression of IL6 and/or other critical proteins only in the relevant cell line, or in viral-infected cells.

RanBP2-mediated translation inhibition of the *IL6-HA* reporter requires both the *IL6* 5′UTR and 3′UTRs

To identify the RanBP2-responsive element in the *IL6-HA* mRNA, we generated several chimeric reporter genes. First, we replaced the *IL6* SSCR with the *major histocompatibility complex* (*MHC*) SSCR, which promotes translation in a RanBP2-dependent manner (Mahadevan *et al*, 2013). Production of protein from this intronless chimeric construct (*MHC-IL6-Δi*) was still elevated after RanBP2-depletion (Figure S1D-F). Of note, slightly more protein was made when comparing *MHC-IL6-Δi* to *IL6-Δi* in control cells, which was likely due to the positive effect of a high 5IMP-scoring SSCR on the mRNA's translation, as described previously (Mahadevan *et al*, 2013). Next, we replaced either the *IL6* 5′UTR or the 3′UTR sequences within the *IL6-1i* construct with the corresponding 5′UTR or 3′UTR sequences of *ftz*, to generate *5F-IL6-1i* (5′UTR swapped) and *IL6-1i-3F* (3′UTR swapped) (Figure 5A). While both chimeras were no longer responsive to RanBP2-depletion, the 5F-IL6-1i construct produced less protein in the RanBP2 knockdown cells, while the IL6-1i-3F produced more protein in the control cells (Figure 5B-C). To validate the 5′UTR result, we swapped this region with the 5′UTR of the human *β-globin* gene (Figure 5A). This new chimera reporter (5βG-IL6-1i) produced even less protein in the control cells and was again no longer responsive to RanBP2 depletion.

These results would suggest that there is a repressive element in the 3′UTR that responds to RanBP2. We are unsure of the role of the 5′UTR. Either it is simply required to initiate translation, and without this boost, regulation of the *IL6* mRNA is abrogated, or that in the absence of the 5′UTR, the 3′UTR supresses translation independently of RanBP2.

To further map the RanBP2-responsive element within the 3′UTR, we generated two additional deletion constructs which lack either the first 110 nucleotides of the *IL6* 3′UTR (*IL6-1i-3del1*) or the last 317 nucleotides (i.e., nucleotides 111-428; *IL6-1i-3del2*) (Figure S3A). Interestingly, more protein was produced from *IL6-1i-3del1* compared to the original construct in both control and RanBP2-depleted cells. Despite this, expression of the protein from the *IL6-1i-3del1* construct still increased in the RanBP2-depleted cells (Figure S3B-C), indicating that the reporter still contained a RanBP2-responsive element. Similarly, the amount of protein generated from *IL6-1i-3del2* increased when compared to the original construct in control cells, however no further increase was seen in RanBP2 knockdown cells (Figure S3B-C). Taken together, these data suggest that the RNA elements that confer RanBP2-dependent supression are located in the region spanning nucleotides 111-428.

The *Let7* binding site within the *IL6* 3′UTR is required for RanBP2-supression of IL6 protein production

Previously it was reported that *Let7a* miRNA directly inhibits expression of IL6 by recognizing a binding site in the *IL6* 3′UTR (Iliopoulos *et al*, 2009; Schulte *et al*, 2011). Moreover, it was demonstrated that RanBP2 is required for *Let7a*-mediated translation suppression (Sahoo *et al*, 2017). Importantly, several members of the *Let7* family of miRNAs are

expressed in U2OS cells (Sohn *et al*, 2012; Liu *et al*, 2014). To determine whether the *Let7* binding site is required for RanBP2-mediated suppression of IL6, we generated a mutant of the *IL6-1i-HA* reporter bearing 4 point mutations in the *Let7* recognition site (*IL6-1i-Let7m-HA*) (Figure 6A). As expected, the *IL6-1i-Let7m-HA* construct produced more protein compared to the *IL6-1i-HA* construct in control cells (Figure 6B-C). In contrast, the level of protein from *IL6-1i-Let7m-HA* was similar to *IL6-1i-HA* in RanBP2-depleted cells (Figure 6B-C). Similar results were obtained in RanBP2-dE3 cells (Figure 6D-E). Note that the level of protein generated from co-transfected H1B-GFP was similar in all the cell lines (Figure 6B-E).

To further confirm these results, we monitored the expression of Renilla *luciferase* reporter plasmids carrying the wild-type 3′UTR of *IL6* (*Luc-IL6*) or a mutant version that lacked the *Let7* binding site (*Luc-IL6-Let7m*) (Schulte *et al*, 2011). These reporters were on plasmids that also contained the Firefly *luciferase* gene, to control for general changes in gene expression. In control U2OS cells we observed that *Let7a* inhibited protein production from the *Luc-IL6* reporter, but did not impact expression from *Luc-IL6-(Let7m)* (Figure 6F), as reported by others (Schulte *et al*, 2011). Importantly, RanBP2-dE3 cells significantly enhanced the expression from the *Luc-IL6* construct either with *Let7a* or scrambled miRNA control, and it eliminated the repression of *Luc-IL6* by *Let7a* (Figure 6F).

These results indicate that RanBP2 represses IL6 expression in part through a *Let7*-mediated translational suppression of the *IL6* mRNA. The fact that the RanBP2-dE3 cells have an overall higher expression of all the *Luc-IL6* constructs, regardless of the presence of a *Let7* binding site, suggests that there may be other RanBP2-sensitive elements in the 3′UTR. It is also curious that the *Luc-IL6* and *Luc-IL6-(Let7m)* reporters are not differentially expressed

(Figure 6F, compare *Luc-IL6* and *Luc-IL6-(Let7m)* with scrambled control miRNAs). This may be due to the fact that for the endogenous *Let7* to supress translation through the *IL6* 3′UTR, it requires the *IL6* 5′UTR.

RanBP-dE3 cells have a general RNAi-silencing defect

Our previous results showing that RanBP2-dependent sumoylation led to a decrease in *Let7*-dependent silencing led us to ask whether these cells were compromised generally for miRNA activity. To determine whether the defect in *Let7* mediated silencing extends to other miRNAs, we transfected U2OS or RanBP2-dE3 cells with miR-644, which is known to repress the expression of GAPDH (Sikand *et al*, 2012). In agreement with the idea that RNAi is generally compromised in RanBP2-dE3 cells, the presence of miR-644 did not lead to a decrease in GAPDH levels in these cells, as it did in the wildtype U2OS cells (Figure 6G). It should be noted that at higher levels, miR-644 does inhibit GAPDH in the mutant cells (data not shown), suggesting that the RNAi pathway is not totally inoperative in these cells but is less active.

RanBP2 regulates IL6 translation by stabilizing of AGO1

We next investigated whether components of the RISC pathway were affected by RanBP2. Previously it had been reported that RanBP2 was required for the degradation of AGO2 (Sahin *et al*, 2014), however in other reports depletion of RanBP2 had no effect on AGO2 levels, but instead promoted the association of miRISC with its target mRNAs (Sahoo *et al*, 2017).

When we measured the levels of AGO1 and AGO2, we noticed a complete absence of AGO1 in the RanBP2-dE3 mutant compared to wildtype cells and a small decrease in AGO2 (Figure 7A), although this last observation was variable between experiments. In contrast, Dicer and GW182 levels did not change (Figure S4). We also detected a drop in AGO1 levels after RanBP2-depletion by shRNA (Figure 7C), and in the HAP1 RanBP2-E3 ins cells compared to unmodified HAP1 cells (Figure 7D). Moreover, expression of the ANE1 mutant RanBP2 in RanBP2-dE3 cells restored AGO1 levels (Figure 7E), correlating with the fact that silencing of *IL6* mRNA is restored in this cell line (Figure 3F). In all these exeriments AGO2 levels were unaffected (Figure 7 C-E). Treating the RanBP2-dE3 cells with the proteasome inhibitor, MG132, restored levels of AGO1 so that its levels were similar between the two cell lines (Figure 7A). AGO2 levels slightly increased after MG132-treatment (Figure 7A). Interestingly, this treatment also increased the levels of the mutant RanBP2 (Figures 7A), suggesting that the 15 amino acid deletion destabilizes this protein. In contrast, MG132-treatment had no major effects on the levels of wildtype RanBP2, α-tubulin or RanGAP1.

Remarkably, RanBP2-dE3 and wildtype cells treated with MG132 had much lower levels of IL6-HA than untreated cells (Figure 7A-B). Furthermore, MG132-treated RanBP2-dE3 and wildtype cells had similar levels of IL6-HA protein (Figure 7A-B), suggesting that when Ago proteins are prevented from degradation, RanBP2-dependent sumoylation was no longer required for IL6 suppression. Notably, this treatment did not alter global translation patterns as the level of expression from other co-transfected reporters (H1B-GFP and Flag-HA-tagged EYFP) were similar across all cell lines and all treatments (Figure 7A).

To confirm that AGO1 stability required RanBP2-dependent sumoylation, we treated cells with cycloheximide to prevent further expression of protein, and then assessed the rate at which the remaining AGO1 degraded. Since levels of AGO1 in RanBP2-dE3 cells were already very low, we monitored the levels of overexpressed Flag-HA-tagged AGO1 (FH-AGO1). Note that the presence of an N-terminal tag is known not to interfere with argonaute protein function (Meister *et al*, 2004). Indeed, we observed that FH-AGO1 had a higher turnover rate in RanBP2-dE3 cells compared to unmodified U2OS cells (Figure 7F-G) and that inhibition of degradation with MG132 eliminated the difference in the levels of FH-AGO1 between these two cell lines (Figure S5).

Finally, we tested whether the lack of silencing in RanBP2-dE3 cells can be overcome by overexpressing AGO1. Indeed, overexpression of FH-AGO1 partially suppressed the expression of IL6-HA protein in these cells when compared to the expression of mutant AGO1 (FH-AGO1$^{K564A/K568A}$) (Figure 7H-I), which does not bind to miRNAs (Boland *et al*, 2011). Expression of FH-AGO1 in control U2OS cells did not further reduce IL6-HA levels, suggesting that endogenous levels of AGO1 are sufficient to suppress IL6-HA expression (Figure 7H-I). Expression of FH-AGO1 had no effect on H1B-GFP expression (Figure 7H) indicating that general translation was not perturbed in these cells.

From these experiments we conclude that RanBP2-dependent sumoylation is required to stabilize AGO1, which in turn acts to suppress the translation of the *IL6-HA* reporter. This is in line with previous studies that have shown that the AGO1 protein strongly interacts with, and regulates the expression of *IL6* mRNA upon *Let7a* overexpression (Iliopoulos *et al*, 2009; Schulte

et al, 2011), and that RanBP2 is required for the *Let7*-mediated suppression of *luciferase* reporter mRNAs (Figure 6 and (Sahoo *et al*, 2017)).

RanBP2 promotes the sumoylation, and inhibits the ubiquitination, of AGO1

When analyzing the overexpression of various versions of FH-AGO1, we noted that RanBP2-dE3 cells accumulated huge amounts of high molecular weight AGO1 that were often confined to the stacking gel (Figure 7J). This suggested that a significant proportion of FH-AGO1 accumulated post-translational modifications in RanBP2-dE3 cells and raised the possibility that in the absence of RanBP2-dependent sumoylation, FH-AGO1 was poly-ubiquitinated and then targeted to the proteasome. This high mobility AGO1 was not seen with the FH-AGO1$^{K564A/K568A}$ mutant (Figure 7J), which does not bind to miRNAs, suggesting that RanBP2 may only affect the post-translational modification of active AGO1.

To identify whether RanBP2 promotes the sumoylation of AGO1, we co-expressed FH-AGO1 with His-tagged SUMO2 (His6-SUMO2). To enhance sumoylation we co-transfected SV5-tagged Ubc9 (V5-Ubc9). Again, note that Ubc9 is the only known SUMO-conjugating E2 enzyme in humans. His6-SUMO2-conjugated FH-AGO1 was purified from denatured cell extracts on a nickel column, which binds to the His tag on the exogenous SUMO2, and the eluate was analyzed using an anti-HA antibody. As we suspected, FH-AGO1 was strongly sumoylated in wildtype U2OS and relatively weakly in RanBP2-dE3 cells (Figure 8A). No FH-AGO1 was seen in the nickel-bound fraction from cells that did not express His6-SUMO2, indicating that the signal was specific to His6-SUMO2-FH-AGO1. When total His-tagged SUMO2 conjugated

proteins were assessed, we saw a modest decrease in RanBP2-dE3 relative to wildtype U2OS cells (Figure 8A).

Next, we wanted to assess the effect of the RanBP2 mutation on AGO1 ubiquitination. We co-expressed FH-AGO1 with His-Myc tagged ubiquitin (His-Myc-Ub) in wildtype and RanBP2-dE3 cells. To ensure that we would capture ubiquitinated intermediates, we inhibited protein degradation with MG132. We then purified ubiquitinated substrates from the cell lysates on a nickel column. In contrast to what we had seen with sumoylation, the level of ubiquitinated FH-AGO1 was 30% higher in RanBP2-dE3 cells compared to wildtype U2OS (Figure 8B). Again, no FH-AGO1 was seen in the nickel-bound fraction from cells that did not express His-Myc-Ub, indicating that the signal was specific. Furthermore, when total ubiquitinated products were blotted for, using antibodies against the His tag, we saw a general increase in ubiquitinated substrates, indicating that the RanBP2-dE3 cells had higher levels of ubiquitinated proteins.

To confirm this last result, we immunoprecipitated exogenously expressed FH-AGO1 from MG132-treated cell lines and blotted for endogenous ubiquitin to visualize ubiquitinated conjugates. Again, the level of ubiquitinated AGO1 increased in RanBP2-dE3 cells by about 30% compared to wildtype U2OS (Figure 8C), even though equal amounts of FH-AGO1 were assessed (Figure 8C).

We next want to ensure that the reason that RanBP2-dE3 cells promoted an increase in ubiquitination was due to the loss of its ability to sumoylate downstream targets, and not some other activity that happened to be disabled by the RanBP2-dE3 mutations, such as binding to RanGAP1. To increase the overall levels of sumoylation in these cells, we overexpressed the V5-Ubc9. Indeed, V5-Ubc9 overexpression resulted in an increase in sumoylated RanGAP1 (Figure

8D), supporting the notion that this protocol did indeed result in an increase in overall sumoylation activity in RanBP2-dE3 cells (Figure 8D). When FH-AGO1 was immunoprecipitated and the level of its ubiquitin-conjugates was assessed by immunostaining, we observed that V5-Ubc9 overexpression reduced overall ubiquitination in RanBP2-dE3 cells (Figure 8D). Thus the overexpression of Ubc9, and the general increase in sumoylation activity, reduced FH-AGO1 ubiquitination even in RanBP2-dE3 cells.

From these experiments we conclude that RanBP2 promotes the sumoylation of AGO1 and inhibits its ubiquitination. Our experiments also suggest that sumoylation inhibits ubiquitination of AGO1. Although our experiments strongly indicate that AGO1 is a direct sumoylation substrate for RanBP2, we cannot rule out the possibility that some intermediate targets exist between RanBP2 and AGO1, though we believe that this is unlikely.

RanBP2 associates with AGO1

Previously it had been reported that RanBP2 directly interacts with AGO2 (Sahoo *et al*, 2017). This would further support the notion that RanBP2 directly sumoylates argonaute proteins. Indeed, we found both RanBP2 and the RanBP2-dE3 mutant in immunoprecipitates of FH-AGO1 (Figure 8C), but not in control immunoprecipitates (FH-EYFP). This suggest that RanBP2 interacts with AGO1 in a manner analogous to AGO2. Interestingly, it was previously reported that this interaction required one of two putative SUMO-interacting motifs (SIMs) that are present in the E3 domain of RanBP2. Although the dE3 mutation deletes part of the first putative SIM, the second putative SIM is still intact. While this interaction would suggest that RanBP2 should bind

to sumoylated argonautes, Sahoo and colleages clearly detected interactions between RanBP2 and unmodified AGO2.

DISCUSSION

The present study is the first to address the role of RanBP2 in the regulation of ANE1-associated cytokines. Until now it remained unclear how the ANE1-associated mutations in RanBP2 might contribute to pathology. Our results indicate that one possible contributing factor is that RanBP2 regulates the expression of at least one ANE1-associated cytokine, IL6. Furthermore, our data suggests that RanBP2 sumoylates AGO1, and thereby prevents its ubiquitination and degradation, allowing AGO1, in conjunction with the *Let7* miRNA, to suppress IL6 expression (Figure 9). In agreement with this model, it is well known that *Let7* is a major regulator of IL6 (Iliopoulos *et al*, 2009; Schulte *et al*, 2011) and that this miRNA regulates inflammation signalling (Lin *et al*, 2017; Brennan *et al*, 2017). Moreover, there is evidence that *Let7* levels change in response to infection (Schulte *et al*, 2011; Ma *et al*, 2012; Mazumder *et al*, 2013; Makkoch *et al*, 2016). From all this, an overall model emerges where upon infection, *Let7* and RanBP2 modulate the inflammation response by downregulating IL6, and potentially other cytokines. A defect in this regulation may cause a hyperinflammatory response that leads to pathology.

Given all this, it remains unclear how ANE1 mutations may affect RanBP2 regulation of the RISC complex. Since a version of RanBP2 that contains three separate ANE1 mutations is still able to restore the repression of AGO1, this may indicate that the mutations may only have an impact in the relevant cell type and/or during infection. This would explain why individuals with these mutations lead a fairly normal life prior to viral infection. The infected cells may contain one or more additional factors that interact with RanBP2 near the region where the ANE1 mutations are located and thus modulate the pathway that we outline in our current work. Moreover, since the disease is only 40% penetrant, other host factors may enhance or disrupt interactions between

this region of RanBP2 and modulators of *IL6* mRNA. Another possibility is that the ANE1 mutations affect some other activity of RanBP2. If this is true, RanBP2 may coordinate several processes that impact the immune response.

Previously, we demonstrated that RanBP2 promotes the translation of mRNAs that contain adenine-depleted SSCRs (Mahadevan *et al*, 2013). That work suggests a model where mRNAs that contain adenine-depleted SSCRs are packaged into mRNPs in the nucleus and that as these complexes complete nuclear export, they interact directly with RanBP2 on the cytoplasmic face of the nuclear pore. This interaction likely promotes an mRNP maturation step, either by allowing proteins to come on or off of the mRNP, and/or by modifying mRNP proteins, and this event is required for the efficient translation of these mRNAs (Mahadevan *et al*, 2013; Palazzo *et al*, 2013; Palazzo & Truong, 2016). It is possible that an analogous mechanism is occurring with the *IL6* mRNA. In this scenario, as newly synthesized *IL6* mRNA exits the nuclear pore, it is actively loaded with *Let7*-bound AGO1 by RanBP2. This is supported by the fact that RanBP2 directly interacts with AGO1 (Figure 8C) and by previous reports that suggested that RanBP2 promotes the association of RISC with target mRNAs (Sahoo *et al*, 2017). Our data would suggest that sumoylation may further stabilize the RISC complex onto the *IL6* mRNA. This model can be tested by determining whether RanBP2 must be anchored to the nuclear pore to effectively silence the *IL6* mRNA. Interestingly, many small RNA pathways (i.e. germ granule small RNAs in *Caenorhabditis elegans* and piRNAs in *Drosophila*, zebrafish and mouse) involve the processing and/or loading of small RNAs onto their target complexes in large phase-separated structures, called nuages or germ granules, that are physically associated with nuclear pores (Voronina *et al*, 2011). Indeed, a recent report demonstrated that RanBP2 was required for piRNA silencing of

transposable elements in *Drosophila* (Parikh *et al*, 2018). These studies lend support to our model that RanBP2 may help to assemble or simply stabilize a repressive complex (i.e. the RISC complex in this case) onto the *IL6* mRNA, after it emerges from the nuclear pore. According to this model, RISC components that accompany mRNAs from the nucleus to the cytoplasm, but fail to be sumoylated, are targeted for ubiquitination and subsequent degradation. This model is consistent with our finding that the FH-AGO1$^{K564A/K568A}$ mutant, which lacks miRNA binding and does not attach to mRNAs, does not appear to be subjected to this type of regulation (Figure 7K). Alternatively, these mutations may remove key lysine residues that are ubiquitinated.

Our previous work demonstrated that the zinc fingers of RanBP2 interact with the adenine-depleted SSCRs of a subset of mRNAs that encode secretory proteins, thereby potentiating their translation (Mahadevan *et al*, 2013). Here, we report that both the 5′UTR and the *Let7a* binding site within 3′UTR of *IL6* mRNA are required for RanBP2-regulation of IL6 protein production, whereas the SSCR of *IL6* mRNA is dispensable. The 5′UTR appears to allow the 3′UTR to repress IL6 in a RanBP2-dependent manner, perhaps by modulating how the *Let7*-binding site is recognized. Our data also indicates that other *cis*-elements may be present in the 3′UTR. We inferred this by the fact that out *luciferase* reporter that contains the *IL6* 3′UTR was upregulated in the RanBP2-dE3 cells compared to unmodified cells and this was independent of the *Let7* binding site. Thus, RanBP2 likely regulates the translation of *IL6* mRNA through an additional element in the 3′UTR. This may also explain why AGO1 overexpression does not fully inhibit IL6 production in RanBP2-dE3 cells (Figure 7H-I). Other *cis*- and *trans*-factors that regulate the *IL6* mRNA are known (Iwasaki *et al*, 2011; Masuda *et al*, 2013; Mino *et al*, 2015; Muller *et al*, 2015; Higa *et al*, 2018), however it is unclear if these are responsive to RanBP2.

These elements and factors all regulate *IL6* mRNA stability, so their connection to RanBP2-based regulation seems unlikely. Future studies will be needed to identify these supplementary elements (in the 5′ and 3′UTR) and their modes of action.

Argonautes are known to be extensively post-translationally modified, especially by ubiquitination (Baumberger *et al*, 2007; Bronevetsky *et al*, 2013; Derrien & Genschik, 2014; Josa-Prado *et al*, 2015; Sahin *et al*, 2014; Chinen & Lei, 2017; Kobayashi *et al*, 2018; Nayak *et al*, 2018). Our data suggests that RanBP2 directly sumoylates AGO1, as it has been previously reported for AGO2 (Sahin *et al*, 2014; Josa-Prado *et al*, 2015; Sahoo *et al*, 2017), and that this sumoylation antagonizes AGO1 ubiquitination. How this would work is unclear at the moment. Sumoylation of a particular lysine residue may prevent the same residue from being ubiquitinated and thus stabilize the protein, as reported in other cases (Desterro *et al*, 1998). Alternatively, sumoylation of AGO1 may mask the binding site of an E3 ubiquitin-ligase or help recruit a ubiquitin protease. We however cannot exclude the possibility that additional sumoylated proteins are required to stabilize AGO1. Previously, it has been reported that sumoylation promotes AGO2 degradation (Sahin *et al*, 2014; Josa-Prado *et al*, 2015), although other reports have suggested that sumoylation is required to load miRNAs into AGO2 (Sahoo *et al*, 2017). Interestingly, the ubiquitination site of *Drosophila* AGO1 (the homolog of human AGO2), K514, which is recognized by the RING-type E3 ubiquitin ligase Iruka (Kobayashi *et al*, 2018), is not conserved within human AGO1, suggesting that AGO1 and AGO2 may have different modes of regulation. These possibilities can be sorted out by mapping the relevant sumoylated and ubiquitinated residues on AGO1 and determining whether mutating these residues disrupts RanBP2 dependent regulation. Uncovering the E3 ubiquitin-ligase would also help to clarify these issues.

MATERIALS AND METHODS

Plasmid constructs

For all expression experiments, pCDNA3.1 plasmid containing the human *insulin* cDNA (Palazzo *et al*, 2007) and human *β-globin* (Akef *et al*, 2013); pEGFP plasmid containing the *H1B-GFP* fusion gene (Contreras *et al*, 2003) were described previously. The *interleukin 6* (*IL6*) gene cloned inside pSPORT6 plasmid was purchased from OpenBiosystems, and various versions of the *IL6* gene including *MHC-IL6-Δi, IL6-1f, IL6-1i, 5F-IL6-1i, 5βG-IL6-1i, IL6-1i-3F, IL6-1i-3del1, IL6-1i-3del2,* and *IL6-1i-Let7m*, were cloned inside the pcDNA 3.1 plasmid and associated mutations were made by restriction-enzyme cloning or site-directed mutagenesis (according to manufacturer's protocol). *GFP-RanBP2-ANE1* in pCDNA3 was a generous gift from A. Hoelz. pIRESneo-*FLAG/HA AGO1* (Addgene plasmid # 10820, FH-AGO1) and pIRESneo-*FLAG/HA EYFP* (Addgene plasmid # 10825, FH-EYFP) were gifts from T. Tuschl (Meister *et al*, 2004). The AGO1 site mutant construct FH-AGO1$^{K564A/568A}$, was constructed from FH-AGO1 by restriction-enzyme-free cloning (van den Ent & Löwe, 2006) using the following primer sequences, K564A/568A-forward primer: ATGTCGCACTTGGTGGCATTAACAACATCCTAG and K564A/568A-reverse primer: TGATCGCGAGGCAGAGGTTGGACAGAGTCTG. The human *His6-SUMO2* (in pcDNA3), *V5-Ubc9* plasmid and *His-Myc-ubiquitin* plasmid were gifts from L. Frappier (Vertegaal *et al*, 2006; Li *et al*, 2010; De La Cruz-Herrera *et al*, 2018). shRNA plasmids (details below) were purchased from Sigma; the *CRISPR/CAS9* plasmid, pSpCas9(BB)-2A-Puro (PX459) V2.0 was a gift from F. Zhang (Addgene plasmid#62988) (Ran *et al*, 2013), and plasmids of Dual Luciferase Reporter Assay (psiCHECK2-Luc-IL6 and psiCHECK2-Luc-IL6-(Let7m), details below) were gifts from J. Vogel (Schulte *et al*, 2011).

Cell culture, cell transfection and lentiviral mediated shRNA knockdown

Cell culture and transfection were carried out as described previously (Gueroussov *et al*, 2010; Mahadevan *et al*, 2013). Briefly, both human osteosarcoma (U2OS) and embryonic kidney 293T (HEK293T) were maintained in Dulbeco's Modified Eagle Medium (DMEM) supplemented with 10% fetal bovine serum, and 1% penicillin-streptomycin (WISENT). HAP1 cells (a gift from Alexio Muise) can be obtained from Horizon Genomics (Vienna, Austria). HAP1 cells were grown in Iscove's modified Dulbecco's medium (IMDM) supplemented with 10% fetal calf serum and 1% penicillin-streptomycin (WISENT). All cells were cultured at 37 °C in a 5% CO_2-humidified incubator. For chemical treatments, MG132 (Sigma) and cycloheximide (CHX) (Sigma) were dissolved in DMSO and used at a final concentration of 10 μM and 100 μM, respectively.

All cells were plated 24 h before transfection and transfected at a confluency of 70-80% using GenJet-OS in vitro transfection reagent for U2OS cells (SignaGen Laboratories, Gaithersburg, MD, USA) or JetPRIME for 293T cells (PolyPlus) or Turbofectin for HAP1 cells (OriGene), following the manufacturer's protocol.

Lentiviral-mediated shRNA knockdown was carried out as described previously (Cui *et al*, 2012) with plasmids encoding shRNA against RanBP2 (shRNA1: TRCN0000003452, shRNA3: TRCN0000003454, Sigma), or control vector (pLK0.1). Briefly, plasmids encoding shRNA were transfected into the HEK293T cells together with the accessory plasmids, VSVG and △8.9, to generate lentivirus carrying specific shRNA plasmids. Lentivirus was harvested from the medium 48 h post-transfection by filtering through a 0.44 μm filter. For infection, lentivirus was applied to U2OS cells with 8 μg/ml hexamethrine bromide. Puromycin was applied to the cell 24 h

post-infection at 2 μg/ml to select for infected cells, and puromycin containing medium was changed every other day. Cell lysates were collected 5 days post-infection to assess the level of knockdown, and the cells were used for various experiments as described.

Immunoblotting and immunoprecipitation

For immunoblotting, various culture cell lines were lysed with lysis buffer containing 50 mM Tris-HCl, 150 mM NaCl, 1% Triton X-100, 1 mM EDTA, and complete protease inhibitor cocktail (Roche), pH 7.4, on ice for 30 min. For immunoprecipitation, whole-cell extracts were collected 24-48 h after transfection and lysed in lysis buffer on ice for 30 min. After centrifugation for 30 min at 13,000 *g*, 4 °C, supernatants were collected and incubated with Protein-G Sepharose beads coupled to specific antibodies for 2-3 h with rotation at 4 °C. The beads were washed 3 times with lysis buffer and bound proteins were eluted by boiling for 10 min in sample buffer containing 50 mM Tris-HCl (pH 6.8), 2% SDS, 10% glycerol, 0.1% bromophenol blue and 1% β-mercaptoethanol. For immunoblot analysis, immunoprecipitates or whole-cell lysates were separated by SDS-PAGE, transferred to nitrocellulose membrane and probed with primary antibodies against HA (HA-7 mouse monoclonal, 1:2000 dilution, Sigma; or rabbit polyclonal, 1:1000 dilution, Sigma), α-tubulin (mouse monoclonalDM1A, 1:1,000 dilution, Sigma), GFP (rabbit polyclonal, 1:1000 dilution, Invitrogen), RanGAP1 (mouse monoclonal, 1:1000 dilution, Santa Cruz), RanBP2 (mouse monoclonal mAb414 1:5000, Cederlane, or rabbit polyclonal, 1:1000 dilution, Abcam), Ubc9 (rabbit polyclonal, 1:1000, Cell Signaling), IL6 (mouse monoclonal, 1:2000 dilution, Abcam), AGO2 (11A9 rat monoclonal, 1:1000 dilution, Millipore), His (mouse monoclonal, 1:1000 dilution, Abcam), or AGO1 (rabbit monoclonal, 1:1000 dilution, Cell Signalling), ubiquitin (rabbit polyclonal, 1:500 dilution, Dako), or GAPDH (rabbit

polyclonal, 1:1000 dilution, ABGENT), GW182 (rabbit polyclonal, 1:1000 dilution, Abcam), Dicer (rabbit polyclonal, 1:1000 dilution, Cell Signaling). Subsequently, the relevant horse radish peroxidase (HRP) conjugated anti-rabbit (1:2000, Cell Signaling) or anti-mouse (1:4000, Cell Signaling) secondary antibody was used. Chemiluminescence luminol reagent (Pierce) and the Versadoc system (Bio-Rad) were used to visualize the blots. ImageJ (NIH) was used for densitometry analysis.

Fluorescent In Situ Hybridization (FISH) and immunofluorescence microscopy

Fluorescence in situ hybridization (FISH) staining was done using DNA specific probes against *IL6* (GTAACATGTGTGAAAGCAGCAAAGAGGCACTGGCAGAAAACAACCTGAAC, 5′ labelled with Alexa546, IDT) at a dilution of 1:500 in 60% formamide hybridization buffer as previously described (Gueroussov *et al*, 2010). Samples were mounted on Fluoromount with 4',6-diamidino-2-phenylindole (DAPI) (Southern Biotechnologies, Birmingham, AL, USA). Immunofluorescence staining was performed as previously described (Gueroussov *et al*, 2010; Cui *et al*, 2012) using antibody against RanGAP1 (mouse monoclonal, 1:250 dilution, Santa Cruz) and a secondary antibody (Alexa647-conjugated donkey anti-mouse polyclonal; 1:1000; Life Technologies, Carlsbad, CA, USA). Microscopy, imaging and nuclear mRNA export quantifications were performed as previously described (Palazzo *et al*, 2007; Gueroussov *et al*, 2010; Mahadevan *et al*, 2013). An epifluorescence microscope on a TI-E inverted Nikon microscope using a 60X phase 2, oil objective and a Coolsnap HQ2 14 bit CCD camera (photometric, Tucson, AZ, USA) controlled using NIS elements Basic Research Microscope Imaging Software (2009) was used to capture all the images. Image exposures varied from 30 ms to 2 s. Data pertaining to total integrated intensity, cytoplasmic/total, and nuclear/total

fluorescence intensity was calculated as previously described (Gueroussov *et al*, 2010) from raw, unprocessed images. Images shown in figures were adjusted for brightness and contrast using the Photoshop (Adobe).

RNA isolation and Northern blotting

After 18–24 h of transfection, total RNA from cultured cells was extracted with Trizol Reagent (Invitrogen) according to the manufacturer's protocol. RNA was separated on a denaturing agarose gel, transferred, and probed for *IL6* and *Tubulin* as previously described (Mahadevan *et al*, 2013).

Generation of the SUMO E3 domain mutants of RanBP2 by CRISPR/Cas9

Genome editing of RanBP2 in U2OS or HAP1 cells was performed as previously described (Moyer & Holland, 2015). In brief, gRNA (5′-GGGCTTTCTGCTCAGCGGT-3′) that targets exon 21 of RanBP2 (Figure 3A) was inserted into PX459 V2.0 plasmid and transfected into U2OS and HAP1 cells with GenJet-OS (SignaGen) and Turbofectin (Origene) respectively according to the manufacturer's instructions. After 48 h of transfection, cells were subjected to transient selection with 2 µg/ml puromycin for 1-2 days to enrich for transfected cells. After puromycin selection, single colonies were grown for 2-4 weeks and then part of the colony was subjected to genomic DNA extraction with lysis buffer (10 mM Tris-HCl, pH 7.5, 10 mM of ethylene diamine tetra-acetic acid, 0.5% of sodium dodecyl sulfate, 10 mM of NaCl, 1 mg/mL of proteinase K) as previously described (Moyer & Holland, 2015). PCR screenings were done using p1F and p1R (p1F sequence: 5′-GAACACTAAATCAGGATGCTAATTCTAG-3′ and p1R sequence: 5′-TCTCTTTCTGCTAGAGCTTTAGCTC-3′) primers to assess for presence of insertions and deletions (InDels) that had been made in the region of interest. Any positive hits from the PCR

screening were further verified by Sanger sequencing. In addition, part of the colony was harvested for western blotting and immunofluorescence analysis of localization and post-translational modification status of RanGAP1 as described in the previous sections.

Dual luciferase reporter assay

For the *IL6* 3′UTR luciferase assay, U2OS and RanBP2-dE3 cells (4x104 cells/well) were seeded in 24-well plates 16 h prior to transfection and transfected with psiCHECK2-Luc-IL6 (100 ng) or psiCHECK2-Luc-IL6-(Let7m) (100 ng) together with 50 nM has-Let7a-5p miRNA (MIMAT0000062, Dharmacon) or miRIDIAN microRNA Mimic Negative Control #1 (CN-001000-01-05, Dharmacon) using JetPRIME reagent (PolyPlus) according to the manufacturer's instructions. Cells were collected 24 h after transfection and luciferase activities were measured with Dual-Luciferase Reporter Assay System (Promega) according to manufacturer's instructions.

Sumoylation and ubiquitylation assay

In vivo AGO1 sumoylation was analysed in U2OS and RanBP2-dE3 cells as previously described (Tatham *et al*, 2009; Shen *et al*, 2017; De La Cruz-Herrera *et al*, 2018). Briefly, U2OS and RanBP2-dE3 cells in 10 cm dishes were transfected with plasmids (2.5 µg each) expressing His6-SUMO2 and V5-Ubc9, together with FLAG/HA-tagged AGO1 (FH-AGO1) proteins (in pIRESneo) or empty plasmid negative control using JetPRIME reagent (PolyPlus) according to the manufacturer's instructions. 24 h after transfection, the cells were harvested, and 10% were lysed in 2X SDS loading buffer (60 mM Tris-HCl pH 6.8, 1% SDS, 100 mM DTT, 5% glycerol) to generate an input sample. 90% of the cells were resuspended in 0.2 mL lysis buffer containing 6 M Guanidinium-HCl, 100 mM K_2HPO_4, 20mM Tris-HCl (pH 8.0), 100 mM NaCl, 0.1% Triton

X-100, and 10 mM Imidazole, and incubated on ice 20 min. Lysates were passed through a 30G needle five times. Purification of the His6-SUMO2 conjugates was performed on 50 µL of Ni^{2+}-NTA agarose beads (Qiagen) prewashed with lysis buffer, and incubated for 2-3 h at room temperature with end-over-end rotation. The beads were washed once with 1 mL of lysis buffer, and three times with 1 mL of wash buffer containing 8 M urea, 0.1 M Na_2HPO_4/NaH_2PO_4 (pH 6.4), 0.01 M Tris-HCl (pH 6.4), 10 mM Imidazole, 10 mM β-mercaptoethanol, and 0.1% Triton X-100 before elution in 2X SDS loading buffer.

To detect conjugates exogenous ubiquitin conjugates, cells were co-transfected with plasmids (2.5 µg each) expressing His-Myc-ubiquitin (Li *et al*, 2010) and FH-AGO1 proteins or control plasmids and were treated with 10 µM MG132 for 7 h before harvesting. Ni^{2+}-purified His6-ubiquitin (Ub) forms of FH-AGO1 followed by western blotting analysis were conducted as described above for the sumoylation assay.

To detect ubiquitin modifications on AGO1, cells were transfected with plasmids (2.5 µg each) expressing FH-AGO1 proteins or FH-EYFP (used as a negative control) and were treated with 10 µM MG132 for 7 h before harvesting. 24 h after transfection, cells were lysed in RIPA buffer (50 mM Tris-HCL, 150 mM NaCl, 1% Triton X-100, 1 mM EDTA, and complete protease inhibitor cocktail (Roche), pH 7.4) for immunoprecipitation. Cell lysates were incubated with Protein-G Sepharose beads coupled to the anti-HA antibody for 2-3 h at 4 °C. The beads were washed three times with RIPA and then processed for immunoblotting.

Statistical analysis

Statistical tests were performed using two-tailed Student's *t*-test to calculate P-values. P-value ≤ 0.05 was considered statistically significant. Results of statistical analysis are included in the corresponding figure legends.

Ribosome fractionation

U2OS and RanBP2-dE3 cells were seeded at a confluency of 50-60% into 15 cm dishes and incubated for 24 h. The cells were then transfected with *IL6-li-HA* plasmid (15 µg) using GenJet-OS (SignaGen). 24 hours post-transfection, cells were treated with 100 µg/mL cycloheximide (Sigma) for 15 minutes, harvested using trypsin with 100 µg/mL cycloheximide, and washed two times in PBS with 100 µg/mL cycloheximide. Cells were then lysed in 1 mL of lysis buffer (20 mM HEPES-KOH (pH 7.4), 5 mM $MgCl_2$, 50 mM KCl, 1% Triton X-100, 100 µg/ml cycloheximide, complete protease inhibitor cocktail (Roche), 1 µL DEPC) for 15 min. The lysates were cleared by centrifugation at 16,000 *g* for 10 min at 4ºC and 400 µL of the lysates were layered over a 20-50% sucrose gradient in polysome buffer (20 mM HEPES-KOH (pH 7.4), 5 mM $MgCl_2$, 125 mM KCl, 100 µg/mL cycloheximide). The solution was centrifuged at 36,000 rpm for 2 h in a SW41Ti rotor (Beckman Coulter) at 4ºC. Gradients were fractionated and absorbance at 254 nm was measured using the Piston Gradient Fractionator (Biocomp) coupled with Bio-Rad EM1 UV monitor following the manufacture's protocol.

RNA was isolated from each fraction using the Trizol reagent (Invitrogen) according to the manufacture's protocol. Fractions representing free RNA, monosome, light polysomes (2-4 ribosomes), medium polysomes (5-7 ribosomes) and heavy polysomes (>8 ribosomes) were identified using the gradient profiles generated and were pooled together. *In vitro* transcribed Renilla *luciferase* mRNA (a final amount of 0.3 ng after pooling) was spiked into the fractions

before RNA extraction as an external control. The RNA samples were treated with DNase I (Invitrogen), reversed transcribed into cDNA with SuperScript™ III Reverse Transcriptase (Invitrogen), analyzed by RT-qPCR (Applied Biosystems™ SYBR Green master mix) as per manufacture's protocol. Primers used for RT-qPCR were, *α-tubulin* forward: CCAAGCTGGAGTTCTCTA; reverse: AATCAGAGTGCTCCAGGG; *IL6* forward: TGAGAGTAGTGAGGAACAAG; reverse: CGCAGAATGAGATGAGTTG; and Renilla *luciferase* forward: ATAACTGGTCCGCAGTGGTG; reverse: TAAGAAGAGGCCGCGTTACC. RT-qPCR data was analyzed using the ΔCT method where the relative expression of *IL6* and *tubulin* were normalized to that of Renilla *luciferase*.

miRNA titration assay

U2OS and RanBP2-dE3 cells were seeded at a confluency of 20% in 6-well plates ($0.3x10^6$ cells/well) and incubated for 24 h. The cells were then transfected with 48, 24, 12, or 6 pmol of miR-644 Mimic (Dharmacon) or miRIDIAN miR-144 Mimic (Dharmacon) as a negative control using JetPRIME reagent (PolyPlus) according to the manufacturer's instructions. Cell lysates were collected 48 h after transfection, proteins were separated by SDS-PAGE and immunoblotted for RanGAP1, GAPDH, and α-tubulin.

Acknowledgements

We would like to thank J. Claycomb and C. Smibert for valuable discussions concerning the work in the paper. We would like to thank L. Frappier, J. Vogel, T. Tuschl, F. Zhang for plasmids. This work was funded by a CIHR grant to A. F. Palazzo (FRN 102725).

Author Contributions

All experiments were conceived and designed by Q. Shen, M. Truong, K. Mahadevan, Y.E. Wang, J. Wu and A.F. Palazzo. The experiments were performed by Q. Shen, M. Truong, K. Mahadevan, Y.E. Wang, and J. Wu. The manuscript was written by Q. Shen and A.F. Palazzo.

Conflicts of Interest

The authors declare no conflict of interest. The funding sponsors had no role in the design of the study, in the collection, analyses, or interpretation of data, in the writing of the manuscript, and in the decision to publish the results.

References:

Akef A, Zhang H, Masuda S & Palazzo AF (2013) Trafficking of mRNAs containing ALREX-promoting elements through nuclear speckles. *Nucleus* **4:** 326–340

Akiyoshi K, Hamada Y, Yamada H, Kojo M & Izumi T (2006) Acute necrotizing encephalopathy associated with hemophagocytic syndrome. *Pediatr. Neurol.* **34:** 315–318

Baumberger N, Tsai C-H, Lie M, Havecker E & Baulcombe DC (2007) The Polerovirus silencing suppressor P0 targets ARGONAUTE proteins for degradation. *Curr. Biol.* **17:** 1609–1614

Boland A, Huntzinger E, Schmidt S, Izaurralde E & Weichenrieder O (2011) Crystal structure of the MID-PIWI lobe of a eukaryotic Argonaute protein. *Proc Natl Acad Sci U S A* **108:** 10466–10471

Brennan E, Wang B, McClelland A, Mohan M, Marai M, Beuscart O, Derouiche S, Gray S, Pickering R, Tikellis C, de Gaetano M, Barry M, Belton O, Ali-Shah ST, Guiry P, Jandeleit-Dahm KAM, Cooper ME, Godson C & Kantharidis P (2017) Protective Effect of let-7 miRNA Family in Regulating Inflammation in Diabetes-Associated Atherosclerosis. *Diabetes* **66:** 2266–2277

Bronevetsky Y, Villarino AV, Eisley CJ, Barbeau R, Barczak AJ, Heinz GA, Kremmer E, Heissmeyer V, McManus MT, Erle DJ, Rao A & Ansel KM (2013) T cell activation induces proteasomal degradation of Argonaute and rapid remodeling of the microRNA repertoire. *Journal of Experimental Medicine* **210:** 417–432

Cenik C, Chua HN, Singh G, Akef A, Snyder MP, Palazzo AF, Moore MJ & Roth FP (2017) A common class of transcripts with 5'-intron depletion, distinct early coding sequence features, and N(1)-methyladenosine modification. *RNA* **23:** 270–283

Cenik C, Chua HN, Zhang H, Tarnawsky S, Akef A, Derti A, Tasan M, Moore MJ, Palazzo AF & Roth FP (2011) Genome analysis reveals interplay between 5'UTR introns and nuclear mRNA export for secretory and mitochondrial genes. *PLoS Genetics* **7:** e1001366

Chinen M & Lei EP (2017) Drosophila Argonaute2 turnover is regulated by the ubiquitin proteasome pathway. *Biochemical and Biophysical Research Communications* **483:** 951–957

Contreras A, Hale TK, Stenoien DL, Rosen JM, Mancini MA & Herrera RE (2003) The dynamic mobility of histone H1 is regulated by cyclin/CDK phosphorylation. *Mol. Cell. Biol* **23:** 8626–8636

Cui XA, Zhang H & Palazzo AF (2012) p180 Promotes the Ribosome-Independent Localization of a Subset of mRNA to the Endoplasmic Reticulum. *PLoS Biol* **10:** e1001336

De La Cruz-Herrera CF, Shire K, Siddiqi UZ & Frappier L (2018) A genome-wide screen of Epstein-Barr virus proteins that modulate host SUMOylation identifies a SUMO E3 ligase conserved in herpesviruses. *PLoS Pathog.* **14:** e1007176

Derrien B & Genschik P (2014) When RNA and protein degradation pathways meet. *Front. Plant Sci.* **5:** Available at: https://www.frontiersin.org/articles/10.3389/fpls.2014.00161/full [Accessed December 9, 2018]

Desterro JM, Rodriguez MS & Hay RT (1998) SUMO-1 modification of IkappaBalpha inhibits NF-kappaB activation. *Mol. Cell* **2:** 233–239

van den Ent F & Löwe J (2006) RF cloning: a restriction-free method for inserting target genes into plasmids. *J. Biochem. Biophys. Methods* **67:** 67–74

Forler D, Rabut G, Ciccarelli FD, Herold A, Köcher T, Niggeweg R, Bork P, Ellenberg J & Izaurralde E (2004) RanBP2/Nup358 provides a major binding site for NXF1-p15 dimers at the nuclear pore complex and functions in nuclear mRNA export. *Mol. Cell. Biol* **24:** 1155–1167

Grünwald D & Singer RH (2010) In vivo imaging of labelled endogenous β-actin mRNA during nucleocytoplasmic transport. *Nature* **467:** 604–607

Gueroussov S, Tarnawsky SP, Cui XA, Mahadevan K & Palazzo AF (2010) Analysis of mRNA nuclear export kinetics in mammalian cells by microinjection. *J Vis Exp* **46:** 2387

Higa M, Oka M, Fujihara Y, Masuda K, Yoneda Y & Kishimoto T (2018) Regulation of inflammatory responses by dynamic subcellular localization of RNA-binding protein Arid5a. *Proc. Natl. Acad. Sci. U.S.A.* **115:** E1214–E1220

Hoelz A, Debler EW & Blobel G (2011) The Structure of the Nuclear Pore Complex. *Annual Review of Biochemistry* **80:** 613–643

Ichiyama T, Endo S, Kaneko M, Isumi H, Matsubara T & Furukawa S (2003a) Serum cytokine concentrations of influenza-associated acute necrotizing encephalopathy. *Pediatr Int* **45:** 734–736

Ichiyama T, Isumi H, Ozawa H, Matsubara T, Morishima T & Furukawa S (2003b) Cerebrospinal fluid and serum levels of cytokines and soluble tumor necrosis factor receptor in influenza virus-associated encephalopathy. *Scand. J. Infect. Dis.* **35:** 59–61

Ichiyama T, Nishikawa M, Yoshitomi T, Hayashi T & Furukawa S (1998) Tumor necrosis factor-alpha, interleukin-1 beta, and interleukin-6 in cerebrospinal fluid from children with prolonged febrile seizures. Comparison with acute encephalitis/encephalopathy. *Neurology* **50:** 407–411

Iliopoulos D, Hirsch HA & Struhl K (2009) An epigenetic switch involving NF-κB, Lin28, let-7 microRNA, and IL6 links inflammation to cell transformation. *Cell* **139:** 693–706

Ito Y, Ichiyama T, Kimura H, Shibata M, Ishiwada N, Kuroki H, Furukawa S & Morishima T (1999) Detection of influenza virus RNA by reverse transcription-PCR and proinflammatory cytokines in influenza-virus-associated encephalopathy. *J. Med. Virol.* **58:** 420–425

1 Iwasaki H, Takeuchi O, Teraguchi S, Matsushita K, Uehata T, Kuniyoshi K, Satoh T, Saitoh T, Matsushita M,
2 Standley DM & Akira S (2011) The IκB kinase complex regulates the stability of cytokine-encoding
3 mRNA induced by TLR-IL-1R by controlling degradation of regnase-1. *Nat. Immunol.* **12:** 1167–
4 1175

5 Josa-Prado F, Henley JM & Wilkinson KA (2015) SUMOylation of Argonaute-2 regulates RNA interference
6 activity. *Biochemical and Biophysical Research Communications* **464:** 1066–1071

7 Kansagra SM & Gallentine WB (2011) Cytokine storm of acute necrotizing encephalopathy. *Pediatr.*
8 *Neurol.* **45:** 400–402

9 Kobayashi H, Shoji K, Kiyokawa K, Negishi L & Tomari Y (2018) Iruka Eliminates Dysfunctional Argonaute
10 by Selective Ubiquitination of Its Empty State. *Molecular Cell* Available at:
11 http://www.sciencedirect.com/science/article/pii/S1097276518308931 [Accessed December 9,
12 2018]

13 Li W, You L, Cooper J, Schiavon G, Pepe-Caprio A, Zhou L, Ishii R, Giovannini M, Hanemann CO, Long SB,
14 Erdjument-Bromage H, Zhou P, Tempst P & Giancotti FG (2010) Merlin/NF2 suppresses
15 tumorigenesis by inhibiting the E3 ubiquitin ligase CRL4(DCAF1) in the nucleus. *Cell* **140:** 477–490

16 Lin Z, Ge J, Wang Z, Ren J, Wang X, Xiong H, Gao J, Zhang Y & Zhang Q (2017) Let-7e modulates the
17 inflammatory response in vascular endothelial cells through ceRNA crosstalk. *Scientific Reports* **7:**
18 42498

19 Liu JM, Long XH, Zhang GM, Zhou Y, Chen XY, Huang SH, Liu ZL & Zhang ZH (2014) Let-7g reverses
20 malignant phenotype of osteosarcoma cells by targeting Aurora-B. *Int J Clin Exp Pathol* **7:** 4596–
21 4606

22 Ma Y-J, Yang J, Fan X-L, Zhao H-B, Hu W, Li Z-P, Yu G-C, Ding X-R, Wang J-Z, Bo X-C, Zheng X-F, Zhou Z &
23 Wang S-Q (2012) Cellular microRNA let-7c inhibits M1 protein expression of the H1N1 influenza A
24 virus in infected human lung epithelial cells. *J. Cell. Mol. Med.* **16:** 2539–2546

25 Mahadevan K, Zhang H, Akef A, Cui XA, Gueroussov S, Cenik C, Roth FP & Palazzo AF (2013)
26 RanBP2/Nup358 potentiates the translation of a subset of mRNAs encoding secretory proteins.
27 *PLoS Biol.* **11:** e1001545

28 Makkoch J, Poomipak W, Saengchoowong S, Khongnomnan K, Praianantathavorn K, Jinato T, Poovorawan
29 Y & Payungporn S (2016) Human microRNAs profiling in response to influenza A viruses (subtypes
30 pH1N1, H3N2, and H5N1). *Exp. Biol. Med. (Maywood)* **241:** 409–420

31 Masuda K, Ripley B, Nishimura R, Mino T, Takeuchi O, Shioi G, Kiyonari H & Kishimoto T (2013) Arid5a
32 controls IL-6 mRNA stability, which contributes to elevation of IL-6 level in vivo. *Proc. Natl. Acad.*
33 *Sci. U.S.A.* **110:** 9409–9414

1 Mazumder A, Bose M, Chakraborty A, Chakrabarti S & Bhattacharyya SN (2013) A transient reversal of
2 miRNA-mediated repression controls macrophage activation. *EMBO Rep.* **14:** 1008–1016

3 Meister G, Landthaler M, Patkaniowska A, Dorsett Y, Teng G & Tuschl T (2004) Human Argonaute2
4 mediates RNA cleavage targeted by miRNAs and siRNAs. *Mol. Cell* **15:** 185–197

5 Mino T, Murakawa Y, Fukao A, Vandenbon A, Wessels H-H, Ori D, Uehata T, Tartey S, Akira S, Suzuki Y,
6 Vinuesa CG, Ohler U, Standley DM, Landthaler M, Fujiwara T & Takeuchi O (2015) Regnase-1 and
7 Roquin Regulate a Common Element in Inflammatory mRNAs by Spatiotemporally Distinct
8 Mechanisms. *Cell* **161:** 1058–1073

9 Moyer TC & Holland AJ (2015) Generation of a conditional analog-sensitive kinase in human cells using
10 CRISPR/Cas9-mediated genome engineering. *Methods Cell Biol.* **129:** 19–36

11 Muller M, Hutin S, Marigold O, Li KH, Burlingame A & Glaunsinger BA (2015) A Ribonucleoprotein Complex
12 Protects the Interleukin-6 mRNA from Degradation by Distinct Herpesviral Endonucleases. *PLOS*
13 *Pathogens* **11:** e1004899

14 Nayak A, Kim DY, Trnka MJ, Kerr CH, Lidsky PV, Stanley DJ, Rivera BM, Li KH, Burlingame AL, Jan E,
15 Frydman J, Gross JD & Andino R (2018) A Viral Protein Restricts Drosophila RNAi Immunity by
16 Regulating Argonaute Activity and Stability. *Cell Host & Microbe* **24:** 542-557.e9

17 Neilson DE, Adams MD, Orr CMD, Schelling DK, Eiben RM, Kerr DS, Anderson J, Bassuk AG, Bye AM, Childs
18 A-M, Clarke A, Crow YJ, Di Rocco M, Dohna-Schwake C, Dueckers G, Fasano AE, Gika AD, Gionnis
19 D, Gorman MP, Grattan-Smith PJ, et al (2009) Infection-triggered familial or recurrent cases of
20 acute necrotizing encephalopathy caused by mutations in a component of the nuclear pore,
21 RANBP2. *Am. J. Hum. Genet.* **84:** 44–51

22 Nott A, Le Hir H & Moore MJ (2004) Splicing enhances translation in mammalian cells: an additional
23 function of the exon junction complex. *Genes Dev* **18:** 210–222

24 Palazzo A, Mahadevan K & Tarnawsky S (2013) ALREX-elements and introns: two identity elements that
25 promote mRNA nuclear export. *WIREs RNA* **4:** 523–533

26 Palazzo AF, Springer M, Shibata Y, Lee C-S, Dias AP & Rapoport TA (2007) The signal sequence coding
27 region promotes nuclear export of mRNA. *PLoS Biol* **5:** e322

28 Palazzo AF & Truong M (2016) Single particle imaging of mRNAs crossing the nuclear pore: Surfing on the
29 edge. *Bioessays* **38:** 744–750

30 Parikh RY, Lin H & Gangaraju VK (2018) A critical role for nucleoporin 358 (Nup358) in transposon
31 silencing and piRNA biogenesis in Drosophila. *J. Biol. Chem.* **293:** 9140–9147

32 Pichler A, Gast A, Seeler JS, Dejean A & Melchior F (2002) The nucleoporin RanBP2 has SUMO1 E3 ligase
33 activity. *Cell* **108:** 109–120

1 Ran FA, Hsu PD, Wright J, Agarwala V, Scott DA & Zhang F (2013) Genome engineering using the
2 CRISPR-Cas9 system. *Nat Protoc* **8:** 2281–2308

3 Sahin U, Lapaquette P, Andrieux A, Faure G & Dejean A (2014) Sumoylation of Human Argonaute 2 at
4 Lysine-402 Regulates Its Stability. *PLOS ONE* **9:** e102957

5 Sahoo MR, Gaikwad S, Khuperkar D, Ashok M, Helen M, Yadav SK, Singh A, Magre I, Deshmukh P,
6 Dhanvijay S, Sahoo PK, Ramtirtha Y, Madhusudhan MS, Gayathri P, Seshadri V & Joseph J (2017)
7 Nup358 binds to AGO proteins through its SUMO-interacting motifs and promotes the association
8 of target mRNA with miRISC. *EMBO reports* **18:** 241–263

9 Saitoh H, Pu R, Cavenagh M & Dasso M (1997) RanBP2 associates with Ubc9p and a modified form of
10 RanGAP1. *Proc. Natl. Acad. Sci. U.S.A* **94:** 3736–3741

11 Schulte LN, Eulalio A, Mollenkopf H-J, Reinhardt R & Vogel J (2011) Analysis of the host microRNA
12 response to Salmonella uncovers the control of major cytokines by the let-7 family. *EMBO J* **30:**
13 1977–1989

14 Sell K, Storch K, Hahn G, Lee-Kirsch MA, Ramantani G, Jackson S, Neilson D, von der Hagen M, Hehr U &
15 Smitka M (2016) Variable clinical course in acute necrotizing encephalopathy and identification of
16 a novel RANBP2 mutation. *Brain Dev.* **38:** 777–780

17 Shen Q, Beyrouthy N, Matabishi-Bibi L & Dargemont C (2017) The chromatin remodeling Isw1a complex is
18 regulated by SUMOylation. *Biochem. J.* **474:** 3455–3469

19 Sikand K, Singh J, Ebron JS & Shukla GC (2012) Housekeeping Gene Selection Advisory:
20 Glyceraldehyde-3-Phosphate Dehydrogenase (GAPDH) and β-Actin Are Targets of miR-644a. *PLOS*
21 *ONE* **7:** e47510

22 Singh RR, Sedani S, Lim M, Wassmer E & Absoud M (2015) RANBP2 mutation and acute necrotizing
23 encephalopathy: 2 cases and a literature review of the expanding clinico-radiological phenotype.
24 *European Journal of Paediatric Neurology* **19:** 106–113

25 Sohn EJ, Park J, Kang S & Wu Y-P (2012) Accumulation of pre-let-7g and downregulation of mature let-7g
26 with the depletion of EWS. *Biochem. Biophys. Res. Commun.* **426:** 89–93

27 Tabarki B, Thabet F, Al Shafi S, Al Adwani N, Chehab M & Al Shahwan S (2013) Acute necrotizing
28 encephalopathy associated with enterovirus infection. *Brain Dev.* **35:** 454–457

29 Tatham MH, Rodriguez MS, Xirodimas DP & Hay RT (2009) Detection of protein SUMOylation in vivo. *Nat*
30 *Protoc* **4:** 1363–1371

31 Tisoncik JR, Korth MJ, Simmons CP, Farrar J, Martin TR & Katze MG (2012) Into the eye of the cytokine
32 storm. *Microbiol. Mol. Biol. Rev.* **76:** 16–32

Vertegaal ACO, Andersen JS, Ogg SC, Hay RT, Mann M & Lamond AI (2006) Distinct and overlapping sets of SUMO-1 and SUMO-2 target proteins revealed by quantitative proteomics. *Mol. Cell Proteomics* **5:** 2298–2310

Voronina E, Seydoux G, Sassone-Corsi P & Nagamori I (2011) RNA Granules in Germ Cells. *Cold Spring Harb Perspect Biol* **3:** a002774

Wu X, Wu W, Pan W, Wu L, Liu K & Zhang H-L (2015) Acute Necrotizing Encephalopathy: An Underrecognized Clinicoradiologic Disorder. *Mediators Inflamm* **2015:** Available at: https://www.ncbi.nlm.nih.gov/pmc/articles/PMC4385702/ [Accessed September 8, 2018]

FIGURE LEGENDS

Figure 1. Most ANE1-associated cytokine genes are not depleted of adenines and have low 5IMP scores.

(A) For each gene in the human genome, the longest tract of adenine-less sequence in the first 99 nucleotides of the open reading frame was tabulated as in Palazzo *et al,* 2007, and plotted, with the *x-axis* representing the length of these tracts, and the *y-axis* representing the fraction of genes in each set with these tract lengths. This was tabulated for all genes that contain an SSCR that lacks introns in their 5′UTR ("SSCR 5UI-"; blue), which are known to be positively regulated by RanBP2 (Mahadevan *et al*, 2013), and for genes that lacked SSCRs ("Non-SSCR"; green). To control for the length of adenine-less tracts in random human DNA sequences, the frequency of adenine-less tract length was also tabulated for regions 3 kb upstream (yellow) and 3 kb downstream (red) of protein coding genes. The adenine-less tract lengths for ANE1-associated cytokine genes are labeled. (B) For each gene in the human genome the 5IMP score was calculated, as described in Cenik et al., 2017, and plotted with the *x-axis* representing binned 5IMP scores, and the *y-axis* representing the fraction of genes in each set with these scores. This was tabulated for all genes that contain an SSCR that lacks introns in their 5′UTR ("SSCR 5UI-"; blue), for genes that contain both an SSCR and one or more introns in their 5′UTR ("SSCR 5UI+"; red) and for all genes that contain one or more introns in their 5′UTR ("All Genes 5UI+"; green). The 5IMP scores for ANE1-associated cytokine genes are labeled.

Figure 2. RanBP2 supresses the translation of *IL6* mRNA.

(A) U2OS cells were infected with lentivirus containing shRNA1 or shRNA3 directed against RanBP2, or scrambled shRNA ("control shRNA"). Four days post-infection, cell lysates were collected, separated by SDS-PAGE, and immunoblotted for nucleoporins using mAb414, which recognizes RanBP2, and α-tubulin as a loading control. (B-C) U2OS cells were infected with lentivirus that delivered shRNA1 or shRNA3 against RanBP2 or control virus. Three days post-infection, cells were transfected with plasmids containing either the *IL6-HA*, *insulin-HA*, or *β-globin-HA* genes. 18–24 h post-transfection cell lysates were collected and separated by SDS-PAGE. The level of each protein was analyzed by immunoblot for HA, and α-tubulin as a loading control (B). The levels of each HA-tagged protein and α-tubulin were quantified using densitometry analysis. The HA/tubulin ratio was normalized to control shRNA-treated cells and plotted (C). (D) As in (C) except that cell lysates (left panel) or supernatant precipitated by TCA (right panel) were collected and separated by SDS-PAGE and immunoblotted with antibodies against HA and α-tubulin. (E-F) As in (C-D) except that RNA was purified from cell lysates and separated on a denaturing agarose gel. The levels of *IL6-HA* mRNA and *α-tubulin* were assessed by northernblot, while the ribosomal RNA was detected by ethidium bromide (E). *IL6-HA* and *α-tubulin* mRNA levels were quantified using densitometry analysis. The *IL6-HA*/*tubulin* ratio was normalized to control shRNA-treated cells and plotted (F). (G-H) Control and RanBP2-depleted cells were transfected with *IL6-HA* plasmid for 14-18 hr, then fixed, permeabilized, and stained for mRNA using a fluorescent in situ hybridization (FISH) probe directed against *IL6*. The cells were imaged (G) and total integrated fluorescence was assessed in the cytoplasm and nucleus (H). For each experiment at least 20 cells were assessed with each bar represents the average and SEM of 3 independent experiments. Scale bar = 10 μm. Each bar is the

average of 3 independent experiments ± SEM. *P = 0.01–0.05, **P = 0.001–0.01, ***P < 0.001, n.s. indicates no significant difference (Student's *t*-test).

Figure 3. The SUMO E3-ligase domain of RanBP2 is required for IL6 translational suppression in U2OS cells.

The SUMO E3-ligase domain of RanBP2 was targeted by CRISPR/Cas9 in U2OS cells. (A) A schematic diagram of the region of the RanBP2 gene targeted by CRISPR/Cas9 loaded with the guide RNA, "gRNA-dE3-1#", whose sequence is shown in (B). Also indicated are the PCR amplification primers "p1F" and "p1R", and the regions deleted "f1-del" and "f2-del" in each *RanBP2* allele present in the cell clone "RanBP2-dE3". (C) PCR amplification, using p1F and p1R primers, of the genomic region targeted by gRNA-dE3-1#. Note that the reaction from the RanBP2-dE3 cell clone lysates produced two amplicons ("f1" and "f2"), which were both smaller than the amplicon produced from unmodified wildtype U2OS cells ("WT U2OS"). (D) Sequencing of the two PCR products (f1 and f2) in (C). Note that the length of the deletion in each *RanBP2* gene allele are indicated. (E) WT U2OS and RanBP2-dE3 cells were fixed, immunostained using anti-RanGAP1 antibody and imaged by epifluorescence microscopy. Scale bar = 10 µm. (F-G) Various cell lines (WT U2OS, RanBP2-dE3 and RanBP2-dE3 that stably express GFP-tagged RanBP2 which contains 3 ANE1-associated mutations ("GFP-ANE1")) were transfected with plasmids containing an intronless version of *IL6-HA* (*IL6-Δi-HA*) and *histone 1B-GFP* (*H1B-GFP*). Cell lysates were collected 24 h post-transfection and separated by SDS-PAGE. Proteins were detected with by immunoblot with antibodies against HA, GFP, RanBP2, RanGAP1 and α-tubulin. Note that H1B-GFP was used as a control for transfection and

general mRNA translation while α-tubulin was used as a loading control. Also note that RanBP2-dE3 cells had lower expression of RanBP2 and lacked sumoylated-RanGAP1. This sumoylation pattern was re-established by the expression of GFP-ANE1. Also note that the level of GFP-ANE1 was less than the level of RanBP2 present in WT U2OS cells. IL6-HA and H1B-GFP protein levels were quantified using densitometry analysis and the ratio of IL6-HA/H1B-GFP was normalized to WT U2OS cells. (H-I) The same experiment as in (F-G), except that an intron-containing *IL6-HA* construct (*IL6-1i-HA*) was used. (J-L) WT U2OS, RanBP2-dE3 cells were transfected with an intron-containing *IL6-HA* construct (*IL6-1i-HA*). 24 h later cells were lysed and fractionated by centrifugation over a sucrose gradient. (J) OD254 trace of the sucrose gradients to determine the distribution of monosomes and polysomes. RT-qPCR of *IL6* (K) and *α-tubulin* (L) mRNA normalized against *luciferase* mRNA that was spiked into each fraction to control for RNA recovery. Note the significant increase in *IL6* mRNA in the polysome fraction in RanBP2-dE3 cells. Each bar is the average of 3 independent experiments ± SEM. *P = 0.01–0.05, **P = 0.001–0.01, (Student's *t*-test).

Figure 4. The SUMO E3-ligase domain of RanBP2 is required for IL6 translational suppression in HAP1 cells.

The SUMO E3-ligase domain of RanBP2 was targeted by CRISPR/Cas9 in the haploid human HAP1 cells. (A) A schematic diagram of the region of the *RanBP2* gene targeted by CRISPR/Cas9 loaded with the guide RNA, "gRNA-dE3-1#", whose sequence is shown in Figure 3B. Note that the insertion "ins" in the "RanBP2-E3 ins" cell line is indicated. (B) Sequencing of the single allele of the *RanBP2* gene in RanBP2-E3 ins cells. Note that the allele contained a 51 base pair

insertion just downstream of the PAM sequence of the guide RNA. This insertion corresponds to a 17 amino acid insertion into the SUMO E3-ligase domain of RanBP2. (C-D) Wildtype (WT) HAP1 and RanBP2-E3 ins cells were transfected with plasmids containing an intron-containing version of *IL6-HA* and *H1B-GFP* and then cell lysates were collected 24 h post-transfection. IL6-HA was immunoprecipitated with mouse anti-HA antibody and protein G beads (Sigma), separated by SDS-PAGE and immunoblotted with a rabbit anti-HA antibody (top panel). For the detection of other proteins, cell lysates were directly separated by SDS-PAGE and immunoblotted with antibodies against GFP, RanBP2, RanGAP1 and α-tubulin. Note that RanBP2-E3 ins cells lacked sumoylated-RanGAP1 but expressed RanBP2 at similar levels to WT U2OS cells. IL6-HA and H1B-GFP protein levels were quantified using densitometry analysis and the ratio of IL6-HA/H1B-GFP was normalized to WT U2OS cells. Each bar is the average of 3 independent experiments ± SEM. **P* = 0.01–0.05 (Student's *t*-test).

Figure 5. **The 5′UTR and 3′UTR of *IL6* mRNA are required for the regulation of IL6 protein production by RanBP2.**

(A) Schematic of the *IL6-1i* constructs where the 5′UTR was replaced with that of the *ftz* reporter (*5F-IL6-1i*) or the β-globin reporter (*5βG-IL6-1i*), and the 3′UTR was replaced with that of the ftz reporter (*IL6-1i-3F*). Note that all constructs retain the HA tag. (B-E) Cells treated with lentivirus that delivers shRNA1 against RanBP2, or scrambled shRNA ("control shRNA") were transfected with the various *IL6-1i* constructs. 24 h post-transfection cell lysates were collected and separated by SDS-PAGE. The level of IL6-HA and α-tubulin were analyzed by immunoblot (B, D). The HA/tubulin ratio was quantified using densitometry analysis, normalized to *IL6-1i*-transfected

control shRNA-treated cells, and plotted (C, E). Each bar is the average of 3 independent experiments ± SEM. *P = 0.01–0.05, n.s. indicates no significant difference (Student's t-test).

Figure 6. The *Let7* binding site in the *IL6* 3′UTR is required for its repression by RanBP2-dependent sumoylation.

(A) Schematic representation of *Let7a* complementarity to the 3′UTR of *IL6*, and *IL6-Let7m*, whose *Let7a* binding site contains four point mutations. (B-C) Cells treated with lentivirus that delivers shRNA1 against RanBP2, or scrambled shRNA ("control shRNA") were transfected with the *IL6-1i* or *IL6-1i-Let7m*, which contains the mutations indicated in (A). 24 h post-transfection cell lysates were collected and separated by SDS-PAGE. The level of IL6-HA and α-tubulin were analyzed by immunoblot (B). The HA/tubulin ratio was quantified using densitometry analysis, normalized to IL6-1i-HA transfected control shRNA-treated cells, and plotted (C). Each bar is the average of 3 independent experiments ± SEM. (D-E) WT U2OS, and RanBP2-dE3 cells were transfected with *IL6-1i* or *IL6-1i-Let7m* and *H1B-GFP*. Cell lysates were collected 24 h post-transfection and separated by SDS-PAGE. Proteins were detected with by immunoblot with antibodies against HA, GFP, RanBP2, RanGAP1 and α-tubulin (D). IL6-HA and H1B-GFP protein levels were quantified using densitometry analysis and the ratio of IL6-HA/H1B-GFP was normalized to *IL6-1i-HA* transfected WT U2OS cells (E). (F) WT U2OS, and RanBP2-dE3 cells were co-transfected with *Let7a* miRNA or a scrambled control miRNA ("control miR"), and a dual luciferase plasmid that contains a *Renilla luciferase* reporter plasmid, carrying either the wild-type 3′UTR of *IL6* (*Luc-IL6*) or the *Let7a* binding site mutant (*Luc-IL6-(Let7m*), see Figure 7A for the sequence), and the Firefly *luciferase* as an internal control. 24 h after transfection,

Renilla and Firefly luciferase luminescence were measured and the ratio was normalized to WT U2OS cells transfected with *Luc-IL6* and control miR. (G) WT U2OS, and RanBP2-dE3 cells were transfected with various amounts of miR-644 or 48 pmol of miR-144 ("Ctr miR"). 24 h post-transfection cell lysates were collected, separated by SDS-PAGE, and immunoprobed for GAPDH, RanGAP1 and α-tubulin. Each bar is the average of 3 independent experiments ± SEM. **P* = 0.01–0.05, ***P* = 0.001–0.01, n.s. indicates no significant difference (Student's *t*-test).

Figure 7. RanBP2 represses IL6 expression by promoting AGO1 stabilization.

(A-B) WT U2OS, and RanBP2-dE3 cells were co-transfected with *IL6-1i-HA*, *H1B-GFP* and Flag-His-tagged yellow fluorescent protein (FH-EYFP). 18 h post-transfection, cells were treated with MG132 (10 μM) (MG132 "+"), or DMSO (MG132 "-") for an additional 7 h. Cell lysates were collected, separated by SDS-PAGE, and immunoblotted with antibodies against HA, GFP, AGO2, AGO1, RanGAP1, RanBP2 and α-tubulin. Note that AGO1 and RanGAP1 are blotted together. Also note that DMSO-treated RanBP2-dE3 cells have no detectable AGO1. MG132-treatment led to an increase in AGO1, AGO2 and mutant RanBP2-dE3 levels. In contrast, the same treatment led to a decrease in IL6-HA levels. IL6-HA and H1B-GFP protein levels were quantified using densitometry analysis and the ratio of IL6-HA/H1B-GFP was normalized to DMSO-treated WT U2OS cells (B). (C) U2OS cells treated with shRNA1 against RanBP2 were lysed, separated by SDS-PAGE, and immunoblotted with antibodies against AGO1, AGO2, RanBP2, RanGAP1, and α-tubulin. (D) HAP1 and HAP1 RanBP2-E3 ins cells were lysed, separated by SDS-PAGE, and immunoblotted with antibodies against AGO1, AGO2, RanBP2, RanGAP1, and α-tubulin. (E) WT U2OS, RanBP2-dE3 and RanBP2-dE3 cells which stably

express GFP-RanBP2 with three ANE1 mutations were lysed, separated by SDS-PAGE, and immunoblotted with antibodies against AGO1, AGO2, RanBP2, RanGAP1, and α-tubulin. (F-G) WT U2OS, and RanBP2-dE3 cells were transfected with Flag-HA-tagged AGO1 (FH-AGO1). 24 h post-transfection, the cells were treated with cycloheximide (CHX 100 μM) for various amounts of time to block further translation and thus allowing us to determine the rate of AGO1 turnover. Cell lysates were collected, separated by SDS-PAGE, and immunoblotted with antibodies against HA (FH-AGO1), α-tubulin, RanGAP1 and RanBP2 (F). For each time point, FH-AGO1 and α-tubulin protein levels were quantified using densitometry analysis and the ratio of FH-AGO1/ α-tubulin was normalized to the zero time point (G). (H-I) WT U2OS, and RanBP2-dE3 cells were co-transfected with *IL6-1i-HA*, *H1B-GFP* and either *FH-AGO1*, or *FH-AGO1*$^{K564A/K568A}$. Cell lysates were collected 24 h post-transfection and separated by SDS-PAGE and immunoprobed for IL6-HA (anti HA), H1B-GFP (anti GFP), FH-AGO1 (anti HA), RanBP2, RanGAP1 and α-tubulin proteins (H). H1B-GFP was used as a control for transfection efficiency, and general mRNA translation. α-tubulin was used as a loading control. IL6-HA and H1B-GFP protein levels were quantified using densitometry analysis and the ratio of IL6-HA/H1B-GFP was normalized to FH-EYFP transfected WT U2OS cells (I). (J) WT U2OS, and RanBP2-dE3 cells were transfected with either *FH-AGO1*, *FH-AGO1*$^{K564A/K568A}$ or *FH-EYFP*. Cell lysates were collected 24 h post-transfection, separated by SDS-PAGE and immunoprobed for FH-AGO1, FH-EYFP, RanBP2, RanGAP1, and α-tubulin proteins. Each bar is the average of 3 independent experiments ± SEM. **P* = 0.01–0.05, ***P* = 0.001–0.01, n.s. indicates no significant difference (Student's *t*-test).

Figure 8. RanBP2 promotes the sumoylation and inhibits the ubiquitination of AGO1.

(A) WT U2OS, and RanBP2-dE3 cells were co-transfected with *FH-AGO1*, *V5-Ubc9*, and His-tagged SUMO2 (*His6-SUMO2* "+") or control vector (*His6-SUMO2* "-"). 24 h post-transfection cells were lysed in 6 M guanidinium chloride, and the His6-SUMO2 conjugates were isolated on Nickel beads ("Ni2+ NTA PD") or the lysates were directly analyzed ("input") and separated by SDS-PAGE. Conjugates were analyzed for the presence of FH-AGO1 by immunoblotting for HA (IB: HA), and for total His6-SUMO2 conjugates by immunoblotting for His (IB: His). Relative levels of each signal, as analyzed by densitometry, are indicated below each blot. Input lysates were immunoblotted for FH-AGO1, V5-Ubc9, RanBP2 and α-tubulin. (B) WT U2OS, and RanBP2-dE3 cells were co-transfected with FH-AGO1, and His-Myc-tagged ubiquitin (His-Myc-Ub "+") or as V5-Ubc9 as a control (His-Myc-Ub "-"). 18 h post-transfection, cells were treated with MG132 (10 μM) for an additional 7 h to preserve ubiquitinated conjugates. Cells were lysed in 6 M guanidinium chloride, and the His-Myc-Ub conjugates were isolated on Nickel beads ("Ni2+ NTA PD") or the lysates were directly analyzed ("input") and separated by SDS-PAGE. Conjugates were analyzed for the presence of FH-AGO1 by immunoblotting for HA (IB: HA), and for total His-Myc-Ub conjugates by immunoblotting for His (IB: His). Relative levels of each signal, as analyzed by densitometry, are indicated below each blot. Input lysates were immunoblotted for FH-AGO1, RanBP2 and α-tubulin. (C) WT U2OS, and RanBP2-dE3 cells were transfected with FH-AGO1 or FH-EYFP. 18 h post-transfection, cells were treated with MG132 (10 μM) for an additional 7 h to preserve ubiquitinated conjugates. Cells were lysed in RIPA buffer, and the FH-AGO1/FH-EYFP and associated proteins were isolated by immunoprecipitation using anti-HA antibodies ("IP HA") or the lysates were directly analyzed

("input") and separated by SDS-PAGE. The immuoprecipitates were analyzed for ubiquitinated proteins by immunoblotting against ubiquitin (IB: Ub). They were also analyzed for the immunoprecipitated FH-AGO1/FH-EYFP by immunoblotting against HA, and for co-immunoprecipitated RanBP2. Input lysates were immunoblotted for RanBP2, FH-AGO1 and FH-EYFP (IB: HA) and α-tubulin. (D) WT U2OS, and RanBP2-dE3 cells were transfected with FH-AGO1 and either V5-Ubc9 to enhance sumoylation or control plasmid. 18 h post-transfection, cells were treated with MG132 (10 μM) for an additional 7 h to preserve ubiquitinated conjugates. Cells were lysed in RIPA buffer, and the FH-AGO1/FH-EYFP were isolated by immunoprecipitation using anti-HA antibodies ("IP HA") or the lysates were directly analyzed ("input") and separated by SDS-PAGE. The immuoprecipitates were analyzed for ubiquitinated proteins by immunoblotting against ubiquitin (IB: Ub). Input lysates were immunoblotted for FH-AGO1 (IB: HA), RanBP2, V5-Ubc9, RanGAP1 and α-tubulin. Note that Ubc9 overexpression, rescues RanGAP1-sumoylation in RanBP2-dE3 cells and decreases the amount of ubiquitinated FH-AGO1.

Figure 9. General model for the regulation of *IL6* by RanBP2.

Additional information

Supplementary Information

Figure S1. RanBP2 represses the expression of IL6 independently of splicing and the SSCR

(A) Schematic of the *IL6* constructs tested. This includes an intronless version of *IL6* (*IL6-Δi*), a version containing the first endogenous *IL6* intron (*IL6-1i*) or the *ftz* intron (*IL6-1f*) both inserted at the endogenous first exon-exon boundary. (B-C) U2OS cells were infected with lentivirus that delivered shRNA1 against RanBP2 or control virus. Three days post-infection, cells were transfected with plasmids containing the indicated reporter genes. 18–24 h post-transfection cell lysates were collected and separated by SDS-PAGE. The level of each protein was analyzed by immunoblot for HA, and α-tubulin as a loading control (B). The levels of each HA-tagged protein and α-tubulin were quantified using densitometry analysis. The HA/tubulin ratio was normalized to *IL6-Δi* transfected control shRNA-treated cells and plotted (C). (D) Schematic of the *IL6* constructs tested. This includes a version of *IL6* where the endogenous SSCR was replaced with the mouse *MHC* SSCR derived from the *h2kb* gene (*MHC-IL6-Δi*). (E-F) As performed in (B-C) with each bar being the average of 3 independent experiments ± SEM. *P = 0.01–0.05 (Student's *t*-test).

Figure S2. Localization of RanBP2 variants

(A) WT U2OS, and RanBP2-dE3 cells were fixed and immunostained for RanBP2 and DAPI stained to visualize DNA. Note that the RanBP2-dE3 mutant localizes to the nuclear rim like the unmodified protein. (B) RanBP2-dE3 cells that stably express a GFP-RanBP2 mutant with three

ANE1 mutations was fixed and immunostained for GFP (this was done as the expression of this construct is too low to detect by GFP fluorescence alone) and DAPI stained to visualize DNA. Scale bar = 10 μm.

Figure S3. The RanBP2-responsive element is found in the 3′ end of the *IL6* 3′UTR

(A) Schematic of the *IL6-1i*, *IL6-1i-3del1*, and *IL6-1i-3del2* constructs. 3del1 consists of the deletion of first 1-110 nucleotides of the *IL6* 3′UTR whereas 3del2 consists of the deletion of 111-439 nucleotides of the *IL6* 3′UTR. (B-C) Control and RanBP2 knockdown cells were transfected with HA-tagged *IL6-1i*, *IL6-1i-3del1*, and *IL6-1i-3del2* constructs. Cellular lysates were collected 24 h post-transfection, separated by SDS-PAGE and immunoprobed for IL6-HA and α-tubulin (B). The ratio of IL6-HA relative to tubulin was quantified using densitometry then normalized to control shRNA-treated cells transfected with *IL6-1i* (n = 4, mean ± SEM, **P* = 0.01–0.05 NS indicates no significant (Student's *t*-test)) (C).

Figure S4. RanBP2 is not required for the stability of GW182 and Dicer

WT U2OS, and RanBP2-dE3 cells were co-transfected with *IL6-1i-HA*, and *H1B-GFP*. 18 h post-transfection, cell lysates were collected, separated by SDS-PAGE, and immunoblotted with antibodies against HA, GFP, Dicer, GW182, RanGAP1, RanBP2 and α-tubulin.

Figure S5. RanBP2 stabilizes overexpressed FH-AGO1

(A-B) WT U2OS, and RanBP2-dE3 cells were co-transfected with *FH-AGO1* and *H1B-GFP.* 18 h post-transfection cells were treated with cycloheximide (CHX, 100 μM) in the presence of MG132 (10 μM) or DMSO for 7 hr. Cell lysates were collected, separated by SDS-PAGE, and immunoblotted with antibodies against HA, GFP, AGO2, RanBP2 and α-tubulin (A). FH-AGO1 and H1B-GFP protein levels were quantified using densitometry analysis and the ratio of FH-AGO1/H1B-GFP was normalized to DMSO-treated WT U2OS cells (B). Each bar is the average of 3 independent experiments ± SEM. $^{*}P = 0.01–0.05$, $^{**}P = 0.001–0.01$, n.s. indicates no significant difference (Student's *t*-test).

1

2

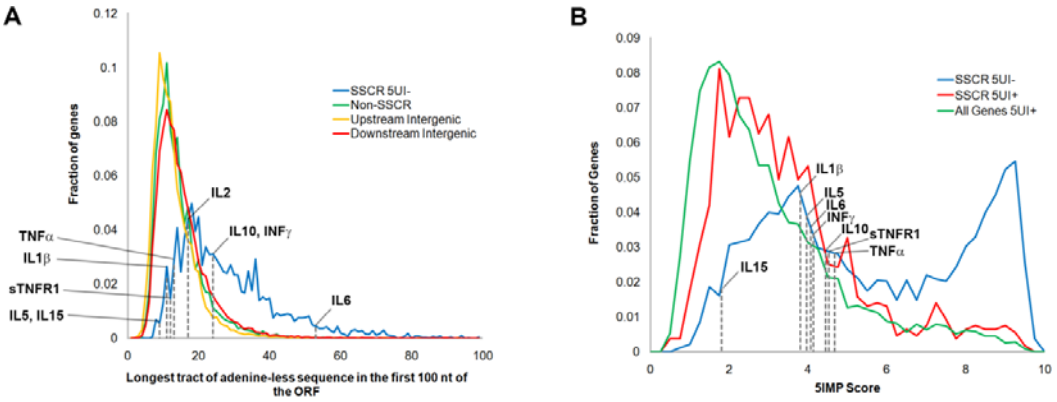

3

4

5 **Figure 1**

6

7

8

1

2

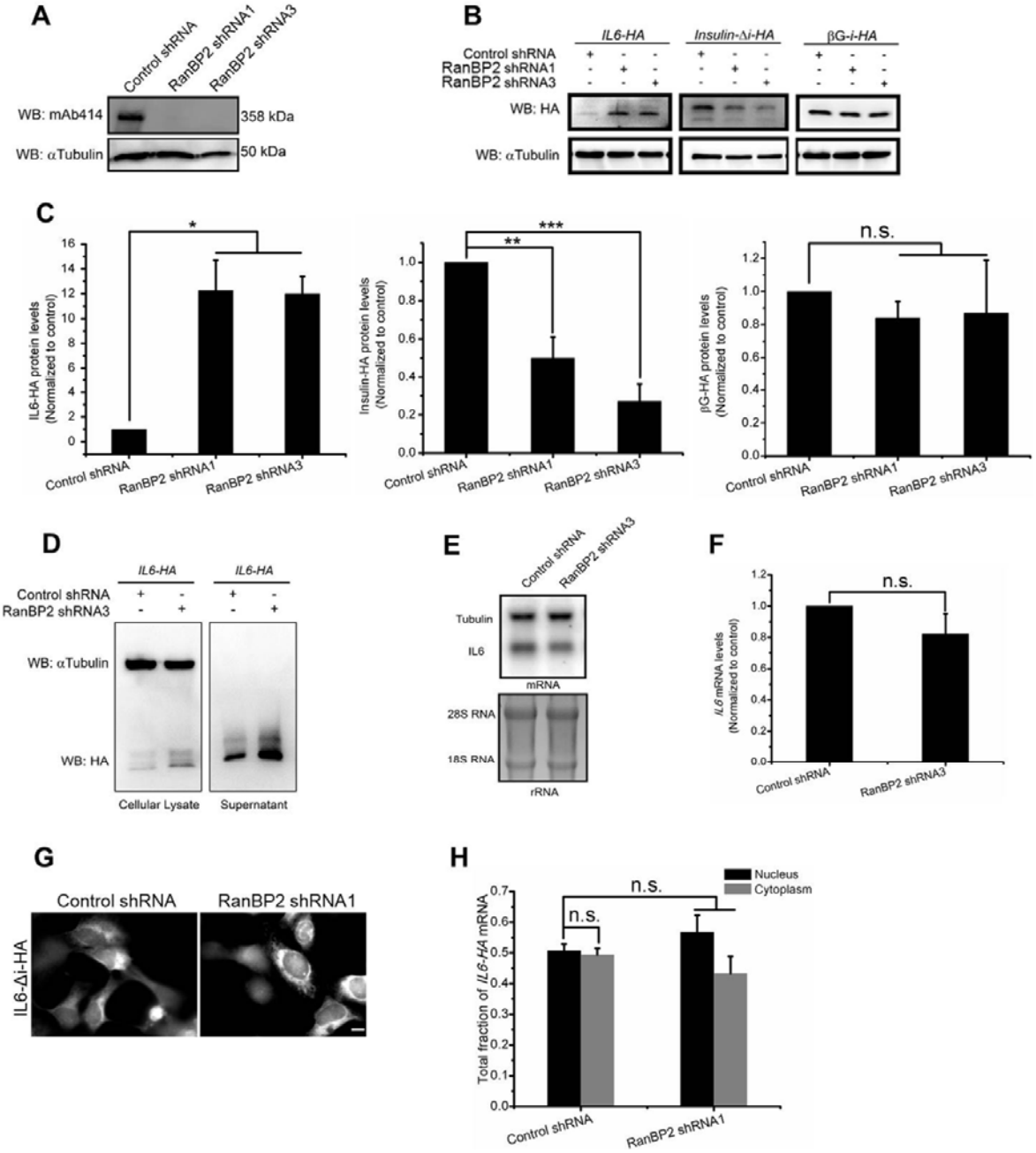

3

4

5 **Figure2**

6

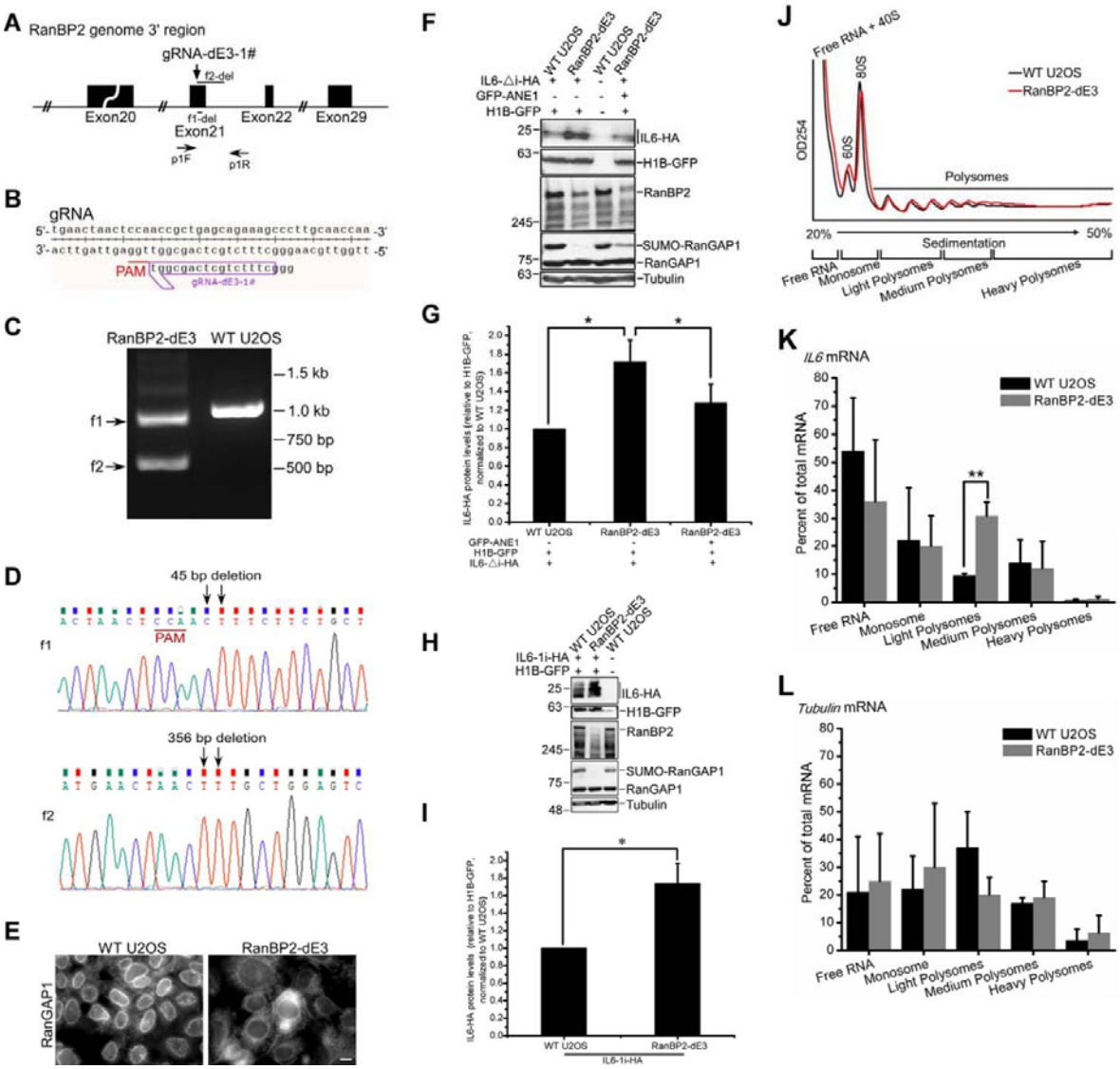
A
RanBP2 genome 3' region
gRNA-dE3-1#
f2-del
Exon20
f1-del
Exon21
Exon22
Exon29
p1F
p1R
B
gRNA
PAM
gRNA-dE3-1#
C
RanBP2-dE3
WT U2OS
1.5 kb
1.0 kb
750 bp
500 bp
f1
f2
D
45 bp deletion
PAM
f1
356 bp deletion
f2
E
WT U2OS
RanBP2-dE3
RanGAP1
F
WT U2OS
RanBP2-dE3
IL6-△i-HA
GFP-ANE1
H1B-GFP
IL6-HA
H1B-GFP
RanBP2
SUMO-RanGAP1
RanGAP1
Tubulin
G
IL6-HA protein levels (relative to H1B-GFP, normalized to WT U2OS)
WT U2OS
RanBP2-dE3
GFP-ANE1
H1B-GFP
IL6-△i-HA
H
IL6-1i-HA
H1B-GFP
IL6-HA
H1B-GFP
RanBP2
SUMO-RanGAP1
RanGAP1
Tubulin
I
IL6-HA protein levels (relative to H1B-GFP, normalized to WT U2OS)
WT U2OS
RanBP2-dE3
IL6-1i-HA
J
Free RNA + 40S
80S
60S
OD254
WT U2OS
RanBP2-dE3
Polysomes
20%
Sedimentation
50%
Free RNA
Monosome
Light Polysomes
Medium Polysomes
Heavy Polysomes
K
IL6 mRNA
WT U2OS
RanBP2-dE3
Percent of total mRNA
Free RNA
Monosome
Light Polysomes
Medium Polysomes
Heavy Polysomes
L
Tubulin mRNA
WT U2OS
RanBP2-dE3
Percent of total mRNA
Free RNA
Monosome
Light Polysomes
Medium Polysomes
Heavy Polysomes

Figure 3

1

2

3

4

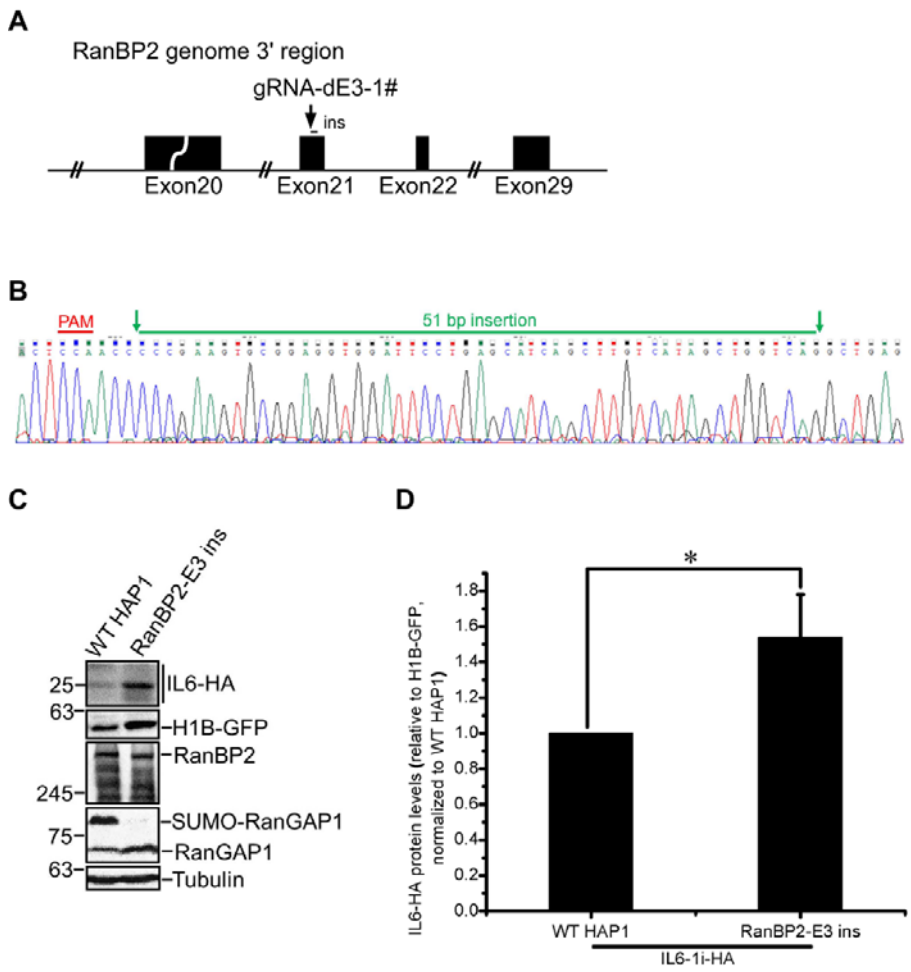

5

6

7

8 **Figure 4**

9

1

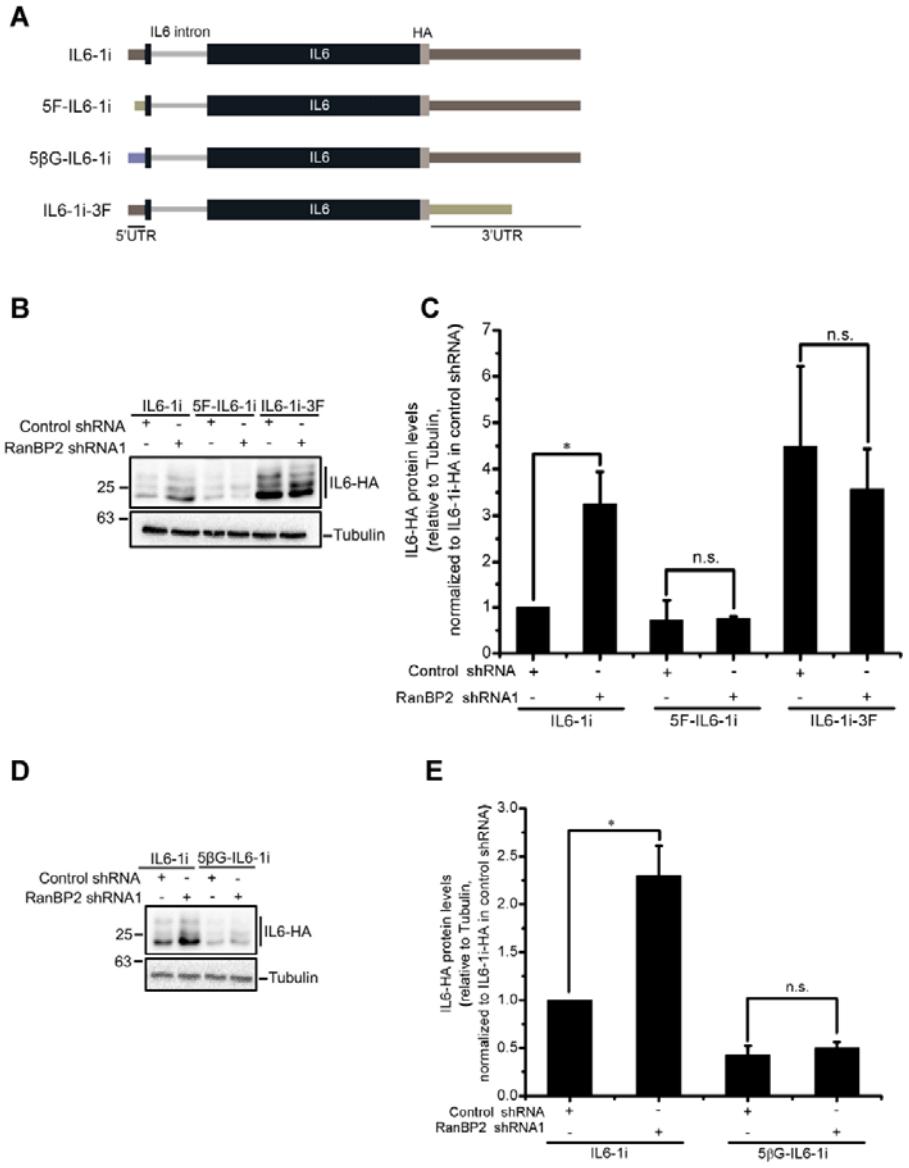

2

3 **Figure 5**

4

5

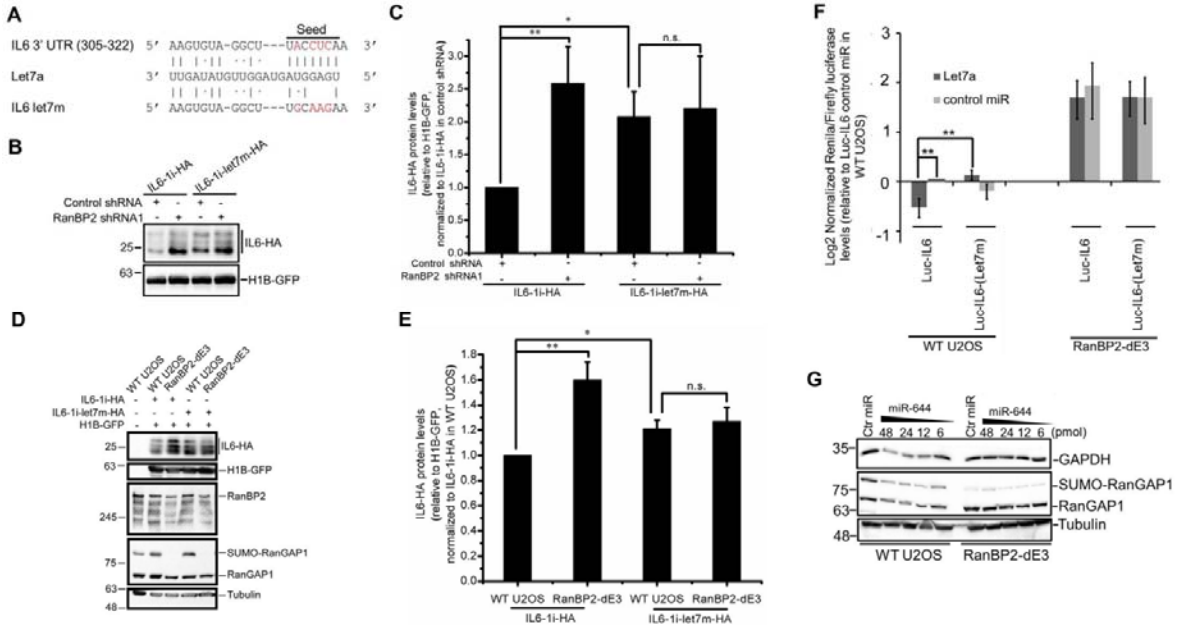
A
Seed
IL6 3' UTR (305-322) 5' AAGUGUA-GGCU---UACCUCAA 3'
Let7a 3' UUGAUAUGUUGGAUGAUGGAGU 5'
IL6 let7m 5' AAGUGUA-GGCU---UGCAAGAA 3'
B
IL6-1i-HA
IL6-1i-let7m-HA
Control shRNA
RanBP2 shRNA1
IL6-HA
H1B-GFP
C
IL6-HA protein levels (relative to H1B-GFP, normalized to IL6-1i-HA in control shRNA)
n.s.
IL6-1i-HA
IL6-1i-let7m-HA
D
WT U2OS
RanBP2-dE3
RanBP2
SUMO-RanGAP1
RanGAP1
Tubulin
E
IL6-HA protein levels (relative to H1B-GFP normalized to IL6-1i-HA in WT U2OS)
F
Let7a
control miR
Log2 Normalized Renilla/Firefly luciferase levels (relative to Luc-IL6 control miR in WT U2OS)
Luc-IL6
Luc-IL6-(Let7m)
G
Ctr miR
miR-644
(pmol)
GAPDH

Figure 6

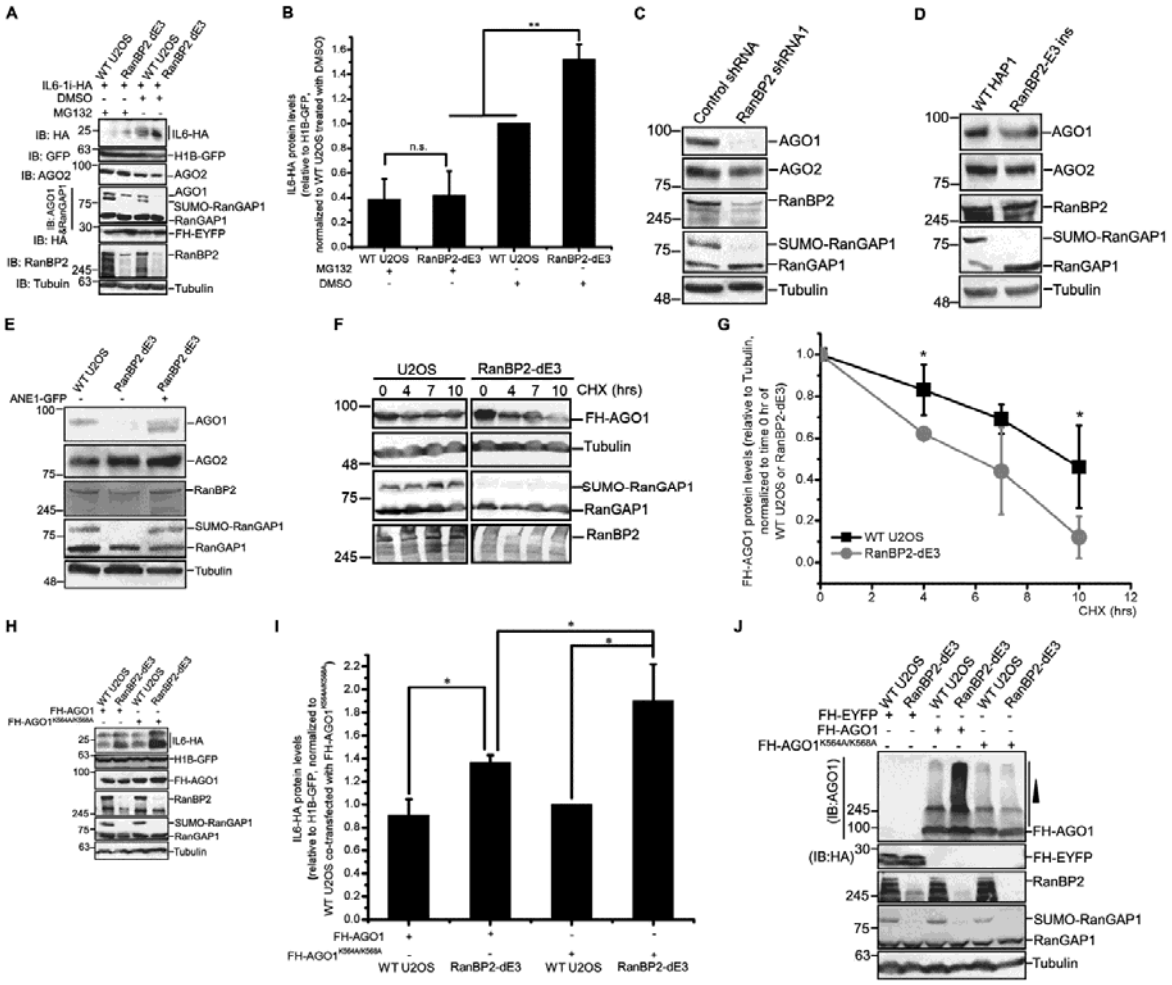

1

2

3 **Figure 7**

4

5

1

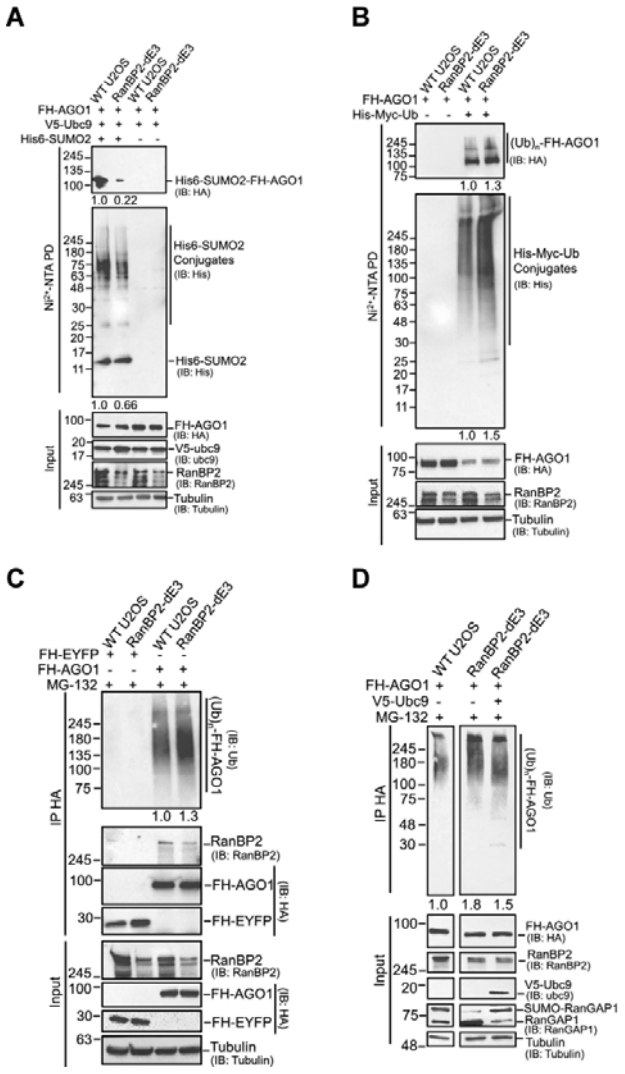

2

3 **Figure 8**

4

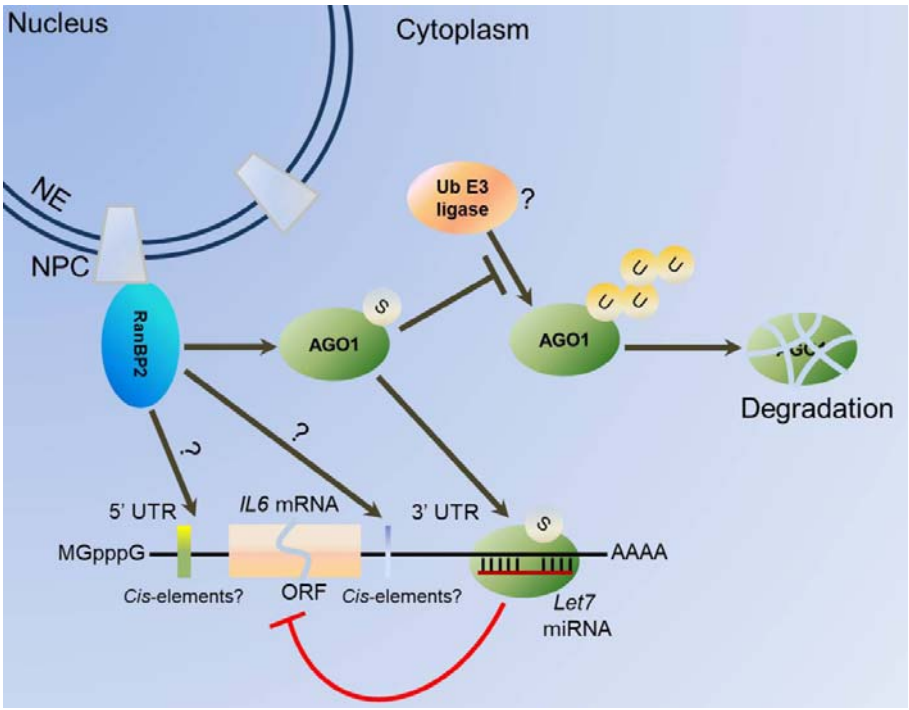
Nucleus
Cytoplasm
NE
NPC
RanBP2
AGO1
S
Ub E3
ligase
?
U
AGO1
Degradation
?
?
5' UTR
IL6 mRNA
3' UTR
MGpppG
AAAA
Cis-elements?
ORF
Cis-elements?
Let7
miRNA

Figure 9

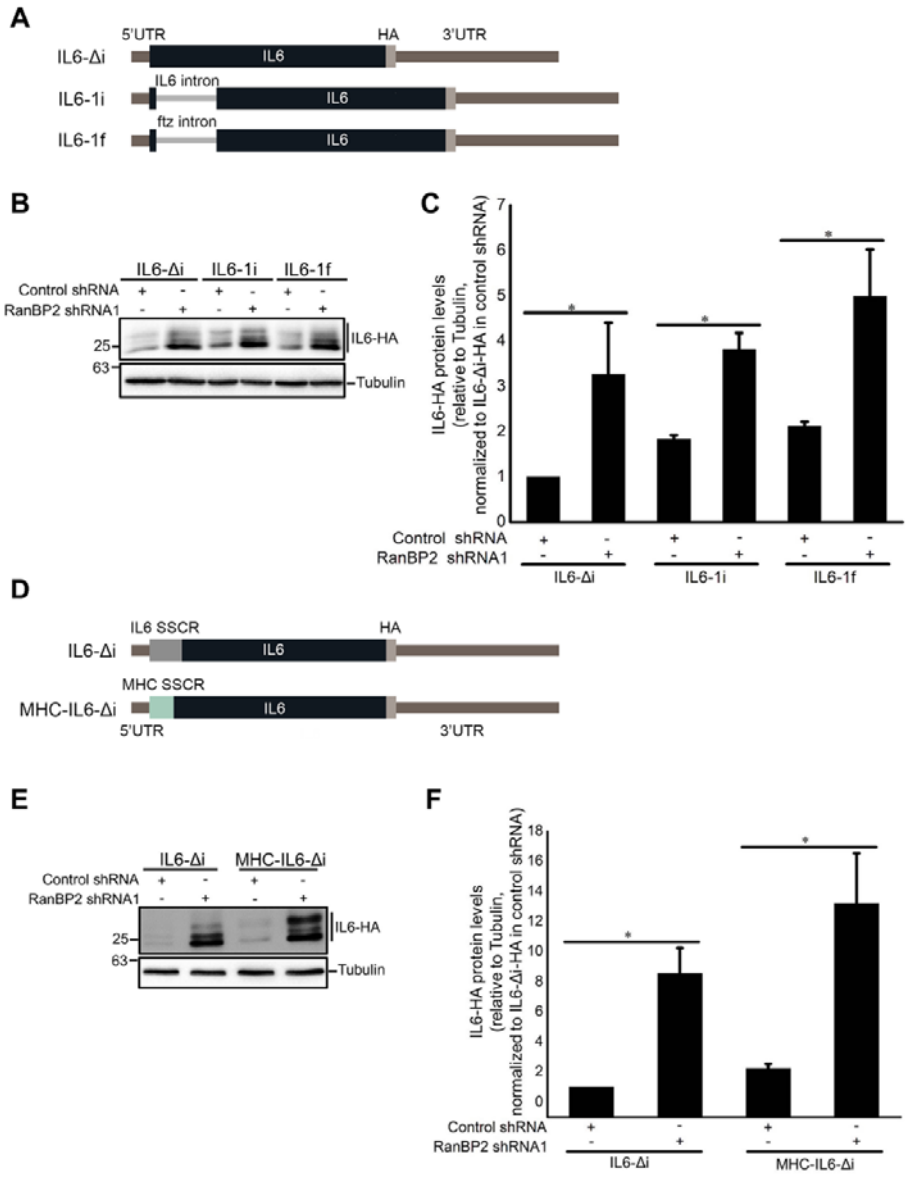
A
5'UTR
HA
3'UTR
IL6-Δi
IL6
IL6 intron
IL6-1i
IL6
ftz intron
IL6-1f
IL6
B
IL6-Δi
IL6-1i
IL6-1f
Control shRNA
RanBP2 shRNA1
25
63
IL6-HA
Tubulin
C
IL6-HA protein levels
(relative to Tubulin,
normalized to IL6-Δi-HA in control shRNA)
Control shRNA
RanBP2 shRNA1
IL6-Δi
IL6-1i
IL6-1f
D
IL6 SSCR
HA
IL6-Δi
IL6
MHC SSCR
MHC-IL6-Δi
IL6
5'UTR
3'UTR
E
IL6-Δi
MHC-IL6-Δi
Control shRNA
RanBP2 shRNA1
25
63
IL6-HA
Tubulin
F
IL6-HA protein levels
(relative to Tubulin,
normalized to IL6-Δi-HA in control shRNA)
Control shRNA
RanBP2 shRNA1
IL6-Δi
MHC-IL6-Δi

Figure S1

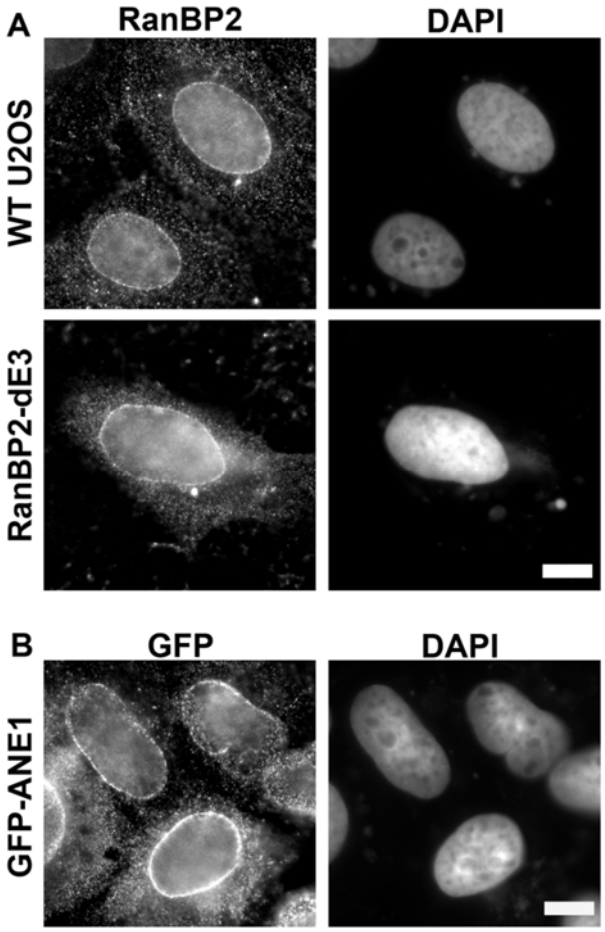

1

2 **FigureS2**

3

4

5

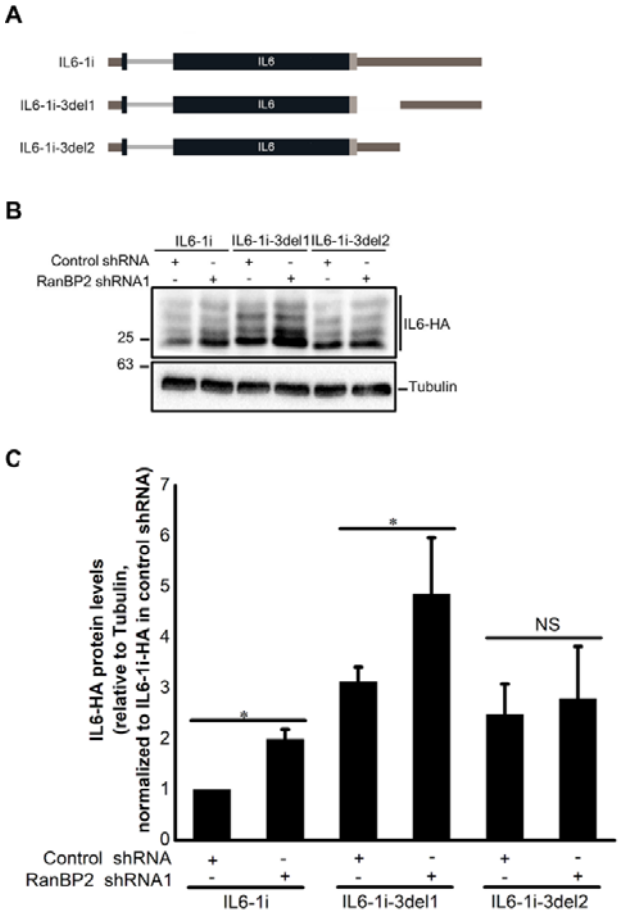
A
IL6-1i
IL6
IL6-1i-3del1
IL6
IL6-1i-3del2
IL6
B
IL6-1i
IL6-1i-3del1
IL6-1i-3del2
Control shRNA
RanBP2 shRNA1
25
63
IL6-HA
Tubulin
C
IL6-HA protein levels
(relative to Tubulin,
normalized to IL6-1i-HA in control shRNA)
NS
Control shRNA
RanBP2 shRNA1
IL6-1i
IL6-1i-3del1
IL6-1i-3del2

Figure S3

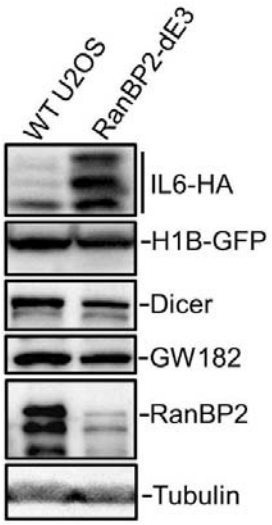

1

2

3 **FigureS4**

4

1

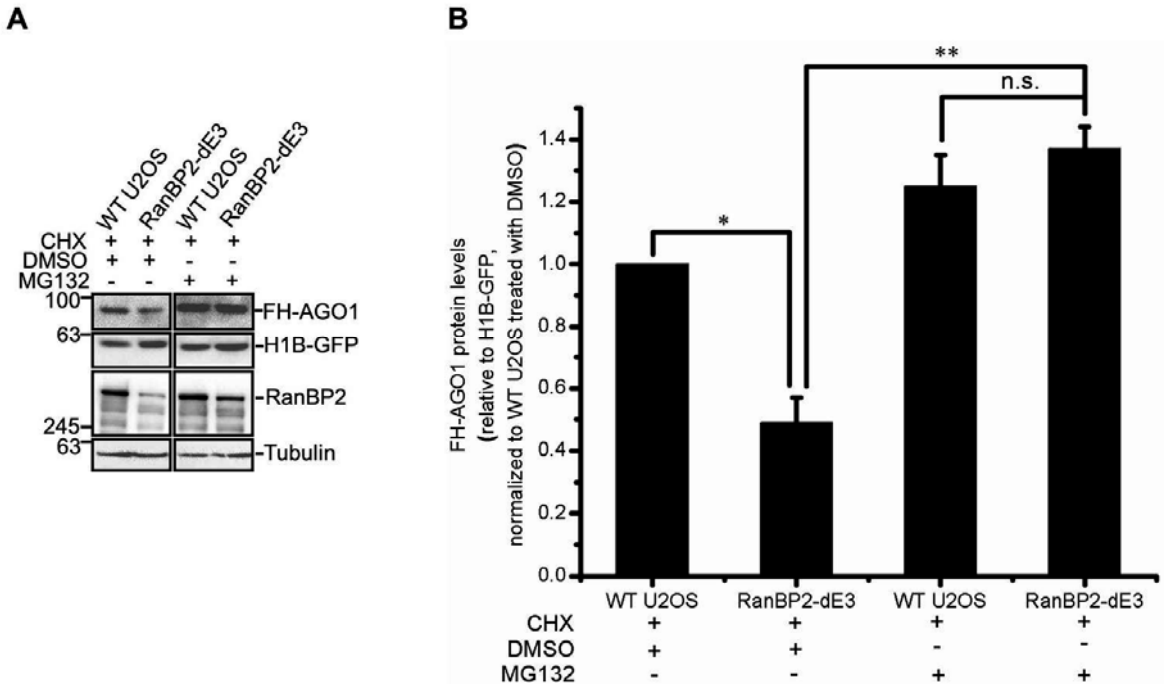

2

3

4

5 **Figure S5**

6

ANE1-associated cytokines	Number of 5'UTR Introns	Reference (Case reports that measured cytokine levels in patients)
IL6	None*	Ichiyama *et al*,1998, Ito *et al*, 1999, Ichiyama *et al*, 2003a, 2003b, Kawada *et al*, 2003, Kubo *et al*, 2006, Akiyoshi *et al*, 2006, Tabarki *et al*, 2013
TNF-α	None	Ichiyama *et al*, 1998, Ichiyama *et al*, 2003a 2003b, Akiyoshi *et al*, 2006, Tabarki *et al*, 2013
IL10	None	Ichiyama *et al*, 2003a, Kubo *et al*, 2006, Kansagra *et al*, 2011
IL15	2	Kubo *et al*, 2006
sTNFR1	None**	Ito *et al*, 1999, Ichiyama *et al*, 2003a 2003b, Kubo *et al*, 2006
IFNγ	None	Ichiyama *et al*, 2003a, Kubo *et al*, 2006
IL1β	1***	Ichiyama *et al*, 1998, Ito *et al*, 1999, Kansagra *et al*, 2011
IL2	None	Kansagra *et al*, 2011
IL5	None****	Kansagra *et al*, 2011

Table1. ANE1-associated cytokines from case reports dating back to 1998

*- The major isoform lacks 5'UTR introns. There are three minor spliced isoforms, one the lacks a 5'UTR intron, one that uses an upstream transcriptional start site and whose extended 5'UTR has an intron, and a third that uses a downstream start codon and has a single 5'UTR intron.

**- The major isoform lacks 5'UTR introns. There are two spliced isoforms that contain the same 5'UTR but have been reported to use different start codons which are found in internal exons. These extended 5'UTRs have two and five introns, respectively.

***- There is a reported minor spliced isoform that has a different 5'UTR which also contains one intron.

****- The major isoform lacks 5'UTR introns. There are three reported minor spliced isoforms, one that lacks 5'UTR introns, and the remaining two with a single 5'UTR intron.